

## RESEARCH ARTICLE

# Yap/Taz-TEAD activity links mechanical cues to progenitor cell behavior during zebrafish hindbrain segmentation

Adrià Voltes<sup>1</sup>, Covadonga F. Hevia<sup>1</sup>, Carolyn Engel-Pizcueta<sup>1</sup>, Chaitanya Dingare<sup>2</sup>, Simone Calzolari<sup>1,\*</sup>, Javier Terriente<sup>1,\*</sup>, Caren Norden<sup>3</sup>, Virginie Lecaudey<sup>2</sup> and Cristina Pujades<sup>1,‡</sup>

## ABSTRACT

Cells perceive their microenvironment through chemical and physical cues. However, how the mechanical signals are interpreted during embryonic tissue deformation to result in specific cell behaviors is largely unknown. The Yap/Taz family of transcriptional co-activators has emerged as an important regulator of tissue growth and regeneration, responding to physical cues from the extracellular matrix, and to cell shape and actomyosin cytoskeletal changes. In this study, we demonstrate the role of Yap/Taz-TEAD activity as a sensor of mechanical signals in the regulation of the progenitor behavior of boundary cells during zebrafish hindbrain compartmentalization. Monitoring of *in vivo* Yap/Taz activity during hindbrain segmentation indicated that boundary cells responded to mechanical cues in a cell-autonomous manner through Yap/Taz-TEAD activity. Cell-lineage analysis revealed that Yap/Taz-TEAD boundary cells decreased their proliferative activity when Yap/Taz-TEAD activity ceased, which preceded changes in their cell fate from proliferating progenitors to differentiated neurons. Functional experiments demonstrated the pivotal role of Yap/Taz-TEAD signaling in maintaining progenitor features in the hindbrain boundary cell population.

**KEY WORDS:** Boundaries, Compartments, Mechanical cues, Progenitor cells, Neurons, Hindbrain, Yap/Taz

## INTRODUCTION

Understanding how progenitor cell specification and differentiation are coordinated with morphogenesis to construct a functional brain is a major challenge in developmental neurobiology. In recent years, a growing body of evidence has shown that mechanical signals are fundamental regulators of cell behavior. For example, extracellular matrix (ECM) rigidity, changes in cell shape and the actomyosin cytoskeleton have been found to direct cell behavior in vertebrates through regulation of the downstream effectors of the Hippo pathway: Yap (Yes-associated protein) and Taz (transcriptional co-activator with PDZ-binding motif, also known as Wwtr1; Halder et al., 2012). A major layer of regulation of Yap and Taz occurs at the level of their subcellular distribution, as the activation of Yap and Taz entails their accumulation into the nucleus where they bind to and activate the TEAD transcription factors (Zhao et al., 2008).


Yap and Taz can interpret diverse biomechanical signals and transduce them into biological effects in a manner that is specific to the mechanical stress involved. For example, Yap localization can be regulated by mechanical cues such as ECM rigidity, strain, shear stress, adhesive area or force (Aragona et al., 2013; Benham-Pyle et al., 2015; Calvo et al., 2013; Chaudhuri et al., 2016; Dupont et al., 2011; Elosegui-Artola et al., 2017, 2016; Nakayama et al., 2017; Wada et al., 2011). Yet the role of Yap and Taz, and their regulation by the multitude of physical tissue deformations that occur during brain morphogenesis remain largely unexplored.

The hindbrain undergoes a dynamic self-organization with dramatic morphogenetic changes during embryonic development, during which a sequence of mechanical and architectural checkpoints must occur to assess the final functional tissue outcome. This involves the segmentation of the tissue, which leads to the transitory formation of seven metameres named rhombomeres (r1-r7). Rhombomeres constitute developmental units of gene expression and cell lineage compartments (Fraser et al., 1990; Jimenez-Guri et al., 2010; Kiecker and Lumsden, 2005). This compartmentalization involves the formation of a cellular interface between segments called the hindbrain boundary (Guthrie and Lumsden, 1991). At early stages of hindbrain segmentation, cells at these boundaries express the corresponding rhombomeric markers, exhibit distinct features such as specific gene expression (Letelier et al., 2018), and are devoid of proneural genes. In contrast, neighboring rhombomeric regions undergo neurogenesis in a Notch-dependent manner (Nikolaou et al., 2009). In addition, boundary cells play very important roles during embryonic development. First, when morphological rhombomeric segments arise, boundary cells act as a morphomechanical barrier to prevent cell intermingling: boundary cells behave as an elastic mesh, thanks to the tension generated by the enrichment of actomyosin cable-like structures at their apical side (Calzolari et al., 2014). When boundary flanking regions are actively engaged in neurogenesis, hindbrain boundaries constitute a node for signaling pathways instructing the differentiation and organization of neurons in the neighboring rhombomeres (Cheng et al., 2004; Cooke et al., 2005; Riley et al., 2004; Terriente et al., 2012). Finally, boundary cells provide proliferating progenitors and differentiating neurons to the hindbrain (Peretz et al., 2016). It remains unknown to what extent these distinct functions of boundary cells are intertwined with their cell proliferation and differentiation properties in order to generate a hindbrain with diverse cell types and correct numbers of cells.

We investigated the role of tissue segmentation and mechanical cues in regulating the balance of the progenitor versus the differentiated cell state in the zebrafish embryonic hindbrain, to address how morphogenetic changes are sensed and transduced into specific cell behaviors. We established that boundary cells acted as mechanosensors through Yap/Taz-TEAD activity, which in the hindbrain was restricted to the rhombomeric boundaries. Using cell-lineage analysis, we showed a decrease in the proliferative activity of

<sup>1</sup>Department of Experimental and Health Sciences, Universitat Pompeu Fabra, 08003 Barcelona, Spain. <sup>2</sup>Goethe University, 60438 Frankfurt, Germany. <sup>3</sup>Max Planck Institute of Molecular Cell Biology and Genetics, 01307 Dresden, Germany. <sup>\*</sup>Present address: ZeClinics, 08003 Barcelona, Spain.

<sup>‡</sup>Author for correspondence (cristina.pujades@upf.edu)

 A.V., 0000-0003-3521-0721; C.F.H., 0000-0003-4322-2415; C.D., 0000-0002-5116-4721; J.T., 0000-0002-0426-9862; C.N., 0000-0001-8835-1451; V.L., 0000-0002-8713-3425; C.P., 0000-0001-6423-7451

boundary cells during development that coincided with the decline of Yap/Taz-TEAD activity within this cell population. This decrease in cell proliferation preceded changes in the cell fate; specifically, changes in the transition from progenitor cells to differentiated neurons. Finally, using a combination of functional approaches, we demonstrated that Yap/Taz-TEAD activity was essential for maintaining boundary cells as proliferative progenitors. Based on these data, we propose that mechanical forces within the hindbrain boundaries function as information systems affecting progenitor maintenance and therefore balancing proliferation and differentiation.

## RESULTS

### Hindbrain boundary cells display Yap/Taz-TEAD activity

During hindbrain segmentation, morphological boundaries are visible as shallow indentations on the outside of the neural tube

(Calzolari et al., 2014; Maves et al., 2002). In this study, whole-mount *in situ* hybridization experiments indicated that the hindbrain boundary cells, marked by *rfng* expression (Terriente et al., 2012; Letelier et al., 2018), first appeared at the interface between rhombomeres as early as 18 hpf (Fig. 1A-C; Fig. S1A-D"). These boundary cells displayed different morphological features from rhombomeric cells: they differed in their triangular shape (Gutzman and Sive, 2010) and large apical footprints (see white arrows in Fig. S1E,F, and see r3/r4 green segmented cell in Fig. S1G), compared with spindle-shaped rhombomeric cells that have smaller apical sides (Fig. S1G, r4 blue segmented cell). Boundary cells actively divided during early embryonic development, as evidenced by BrdU incorporation (see white arrowheads in Fig. 1D), anti-pH3 immunostaining (see white arrowheads in Fig. 1E) and live imaging of the embryos (Fig. 1F, see non-magenta cell incurring into the

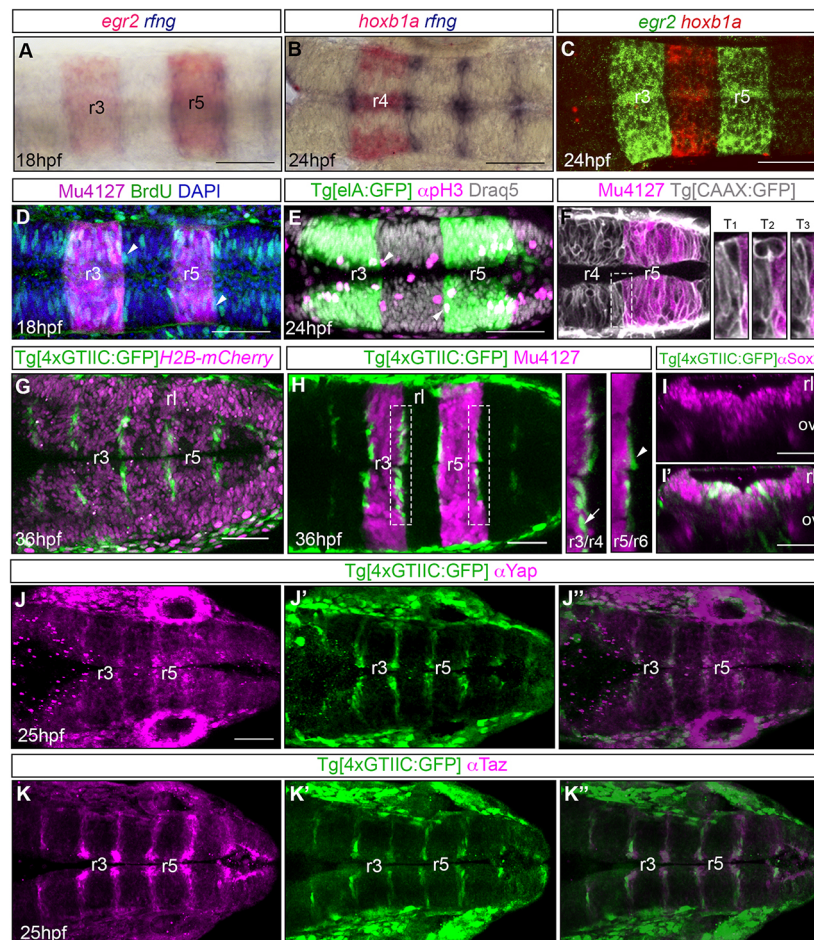


**Fig. 1. Hindbrain boundary cells display Yap/Taz activity.** (A-C) Whole-mount double *in situ* hybridization in embryos at the indicated developmental stages with probes targeting: *egr2a* (A,C), which labels rhombomeres (r) 3 and 5; *hoXB1a* (B,C), which labels r4; and *rfng* (A,B), which labels hindbrain boundaries. The expression of *rfng* is restricted at the interface between adjacent rhombomeres. (D) BrdU staining of a Mu4127 embryo expressing mCherry (magenta) in r3 and r5 at 18 hpf. Cells at the boundaries (at the border of mCherry expression) display green BrdU staining (white arrowheads indicate examples). (E) Immunostaining of a Tg[elA:GFP] embryo at 24 hpf with anti-pH3 (magenta). Nuclei were stained using Draq5 (gray). Cells at the boundaries (at the border of GFP expression) display pH3 staining (see white arrowheads). (F) A still image from a time-lapse analysis of a double transgenic Tg[CAAX:GFP]Mu4127 embryo displaying GFP in the plasma membrane (shown in white) and mCherry in r5 (shown in magenta). T<sub>1</sub>-T<sub>3</sub> are enlargements of the region framed in F, corresponding to different times. Upon division, the cell challenges the boundary when it undergoes mitosis. (G) Tg[4xGTIIC:GFP] embryo injected with H2B-mCherry to visualize cell nuclei, which display Yap/Taz-TEAD activity (green) in discrete progenitor domains of the hindbrain at 36 hpf. Cells of the rhombic lip (rl) are devoid of Yap/Taz activity. (H) Tg[4xGTIIC:GFP]Mu4127 embryos showing that TEAD activity is restricted to the boundary cells. Images on the right are enlargements of the r3/r4 (white arrow indicates a Yap/Taz-active r3 cell) and r5/r6 (white arrowhead indicates an r6 cell with Yap/Taz activity) boundaries framed in H. (I, I') Tg[4xGTIIC:GFP] embryos immunostained using anti-Sox2 antibodies (magenta), showing that green Yap/Taz-TEAD active cells are located in the ventricular zone and express this progenitor cell marker (I'). (J-K'') Whole-mount anti-Yap (J-J'') and anti-Taz (K-K'') immunostaining of Tg[4xGTIIC:GFP] embryos at 25 hpf showing overlapping expression of Yap and Taz (magenta in J, J'', K, K'') with TEAD activity (green cells in J', J'', K', K'') in boundary cells. All images are dorsal views with anterior to the left, except for the transverse views in I', I''. r, rhombomere; rl, rhombic lip; ov, otic vesicle. Scale bars: 50  $\mu$ m.

magenta territory upon mitosis in T<sub>1</sub>-T<sub>3</sub>; Calzolari et al., 2014). Moreover, boundary cells expressed Sox2 (Fig. 1I) supporting the notion that these cells were indeed proliferating neural progenitors (Galant et al., 2016). Interestingly, previous studies showed that boundary cells do not undergo neurogenesis concomitantly with their rhombomeric cell neighbors; accordingly, proneural genes, responsible for driving neurogenesis, are expressed only in zones that flank rhombomere boundaries (Nikolaou et al., 2009).

Boundary cells not only have specific features, but also display distinct functions. We have previously shown that they act as an elastic mesh to prevent cell mixing between adjacent rhombomeres. This mesh is as a result of the assembly of apical actomyosin cable-like structures that generate tension within this cell population (Calzolari et al., 2014). In this respect, given the compelling evidence regarding the relevance of Yap and Taz as downstream mediators of mechanical signals, we aimed to explore whether Yap/Taz-TEAD activity within boundary cells could act as a putative sensor of architectural constraints within the hindbrain boundaries and could convey this information into a specific cell behavior. First, to determine whether Yap and Taz were activators of TEAD transcription factors in these cells, we monitored TEAD activity *in vivo* by using the transgenic zebrafish reporter line Tg[4xGTIIC:GFP], which expresses GFP under the control of four multimerized GTIIC sequences that are consensus TEAD-binding sites (Miesfeld and Link, 2014). Indeed, TEAD activity was confined to discrete territories within the hindbrain (Fig. 1G). These territories coincided with the rhombomeric boundaries, as GFP-expressing cells were found at the interface between two different rhombomeres (Fig. 1H, see insets with magnifications of r3/r4 and r5/r6). Furthermore, boundary TEAD-active cells also expressed Sox2 (Fig. 1I'), demonstrating that they were neural progenitors. Next, we wanted to determine whether the TEAD activity was due to Yap and/or Taz proteins. Although the *yap* transcript is ubiquitously expressed in the embryo (Agarwala et al., 2015), the expression of Yap protein was enriched in hindbrain boundaries (Fig. 1J), and Taz protein was specifically expressed in the boundary cells within the hindbrain (Fig. 1K). As expected, the boundary cells expressing Yap and Taz proteins coincided with cells with TEAD activity (Fig. 1J-J', K-K'). However, the overlap in expression was not perfect most probably due to several scenarios: (1) a difference of levels between the TEAD reporter and Yap/Taz proteins; (2) the expression of Yap and Taz preceded the expression of GFP in the Tg[4xGTIIC:GFP] line; and (3) the GFP of the reporter line was very stable. Nevertheless, most of the boundary cells expressing Yap and Taz do display TEAD activity, supporting the hypothesis that hindbrain boundaries harbor proliferating neural progenitors that are enriched in Yap and Taz proteins and display Yap/Taz-TEAD transcriptional activity.

### Establishment of Yap/Taz-TEAD activity in hindbrain boundary cells

To assess the temporal window of Yap/Taz-TEAD activity in the boundary cells, we monitored its onset by following GFP expression in Tg[4xGTIIC:GFP] embryos (Miesfeld and Link, 2014). Using whole-mount *in situ* hybridization, we found that TEAD activity started by 20 hpf, as transcription of the *gfp* mRNA could be visualized in the boundaries at this stage (Fig. 2A-C). Thus, TEAD-activity occurred not long after hindbrain boundary cells assembled actomyosin-cable structures (15 hpf; Calzolari et al., 2014). GFP-positive boundary cells were detected at a slightly later time point (25 hpf), and GFP expression persisted in the boundaries until 72 hpf (Fig. 2D-G; data not shown). We next analyzed the temporal dynamics of Yap/Taz activity

in the boundary cell population using KAEDE-photoconversion experiments. KAEDE shifts its emission spectrum from green to red after photoconversion, which facilitates the tracing of KAEDE-expressing cells over time (Ando et al., 2002; Hatta et al., 2006; Sapède et al., 2012). We photoconverted the whole population of KAEDE-Yap/Taz-active cells *in vivo* and then traced the photoconverted cell derivatives 18 h or 24 h later (Fig. 2H). To specifically target the Yap/Taz-active cells, we made use of the transgenic line carrying KAEDE under the control of the 4xGTIIC TEAD binding-sites Tg[4xGTIIC:Gal4;UAS:KAEDE]. Photoconversion of green-fluorescent KAEDE (KAEDE<sup>G</sup>) at 30 hpf, resulted in red-fluorescent TEAD-active cells that were born before 30 hpf (Fig. 2I-I'', see no KAEDE<sup>G</sup>-cells in I'). When the same embryos were observed at 48 hpf, the early-born cells were still evident as cells positive for the converted red-fluorescent KAEDE (KAEDE<sup>R</sup>; Fig. 2J,J',J''), but the embryos also displayed cells that were positive for *de novo* synthesized KAEDE<sup>G</sup> (Fig. 2J-J''). A thorough analysis of the KAEDE<sup>G</sup>-positive cells at 48 hpf showed that most of them also expressed KAEDE<sup>R</sup> (compare Fig. 2J',J''), indicating that Yap/Taz-TEAD activity in the hindbrain boundaries was triggered before 30 hpf, as observed in Fig. 2A. When KAEDE was completely photoconverted in 48 hpf embryos (Fig. 2K-K''), no new KAEDE<sup>G</sup>-cells were present at 72 hpf (Fig. 2L') and all the derivatives of Yap/Taz-active cells were KAEDE<sup>R</sup>, suggesting that Yap/Taz-activity was shut off before 48 hpf. Thus, our analysis confirmed that Yap/Taz activity in the hindbrain boundary cells was switched on before 30 hpf, not long after the time at which boundary cells were previously shown to be important as a mechanical barrier (Calzolari et al., 2014). In addition, these results indicated that the Yap/Taz activity strongly decreased before 48 hpf, even though the GFP protein was expressed at later stages (Fig. 2G). Thus, the Tg[4xGTIIC:GFP] line expressed GFP in boundary cells even beyond the time at which the Yap/Taz activity has declined.

### Yap/Taz-TEAD activity senses mechanical inputs in hindbrain boundary cells

Changes in the organization of the actomyosin cytoskeleton have been found to converge on the regulation of Yap and Taz (for reviews, see Halder et al., 2012; Panciera et al., 2017). Our aim was therefore to address whether the integrity of the actomyosin cytoskeleton was necessary for Yap/Taz-TEAD activity within the boundary cells. For this purpose, Yap/Taz-TEAD activity was examined after interference with endogenous tensile forces in the Tg[4xGTIIC:GFP] embryos by several means (Fig. 3): (1) pharmacological inhibition of myosin II or Rock with *para*-nitroblebbistatin or rockout, respectively (Calzolari et al., 2014); (2) disruption of the actomyosin cable by downregulating the function of Rac3b, a small Rho GTPase with a crucial role in the actomyosin-cable assembly in hindbrain boundaries, using a splice-blocking morpholino (Letelier et al., 2018); and (3) conditional inhibition of Rac3b by clonal expression of a dominant-negative form of Rac3b (Myc:hsp:Rac3bDN; Letelier et al., 2018). Both blebbistatin and rockout treatment before the onset of Yap/Taz-TEAD activity within the boundaries resulted in a loss of the activity as shown by *gfp in situ* hybridization analysis (Fig. 3B,C; blebbistatin, *n*=15/20; rockout, *n*=15/19 embryos displaying loss of *gfp* expression in the boundaries), when compared with control embryos incubated in DMSO (Fig. 3A, *n*=2/20 embryos with no *gfp* boundary expression). Thus, treatment with blebbistatin, which inhibits myosin II by blocking the myosin heads in a complex with low actin affinity (Képiró et al., 2014), and treatment with Rockout, which blocks Rho kinase activity (Ernst et al., 2012), led to similar results. A similar loss of Yap/Taz-TEAD activity was observed following downregulation of Rac3b, a small Rho GTPase expressed in hindbrain boundaries

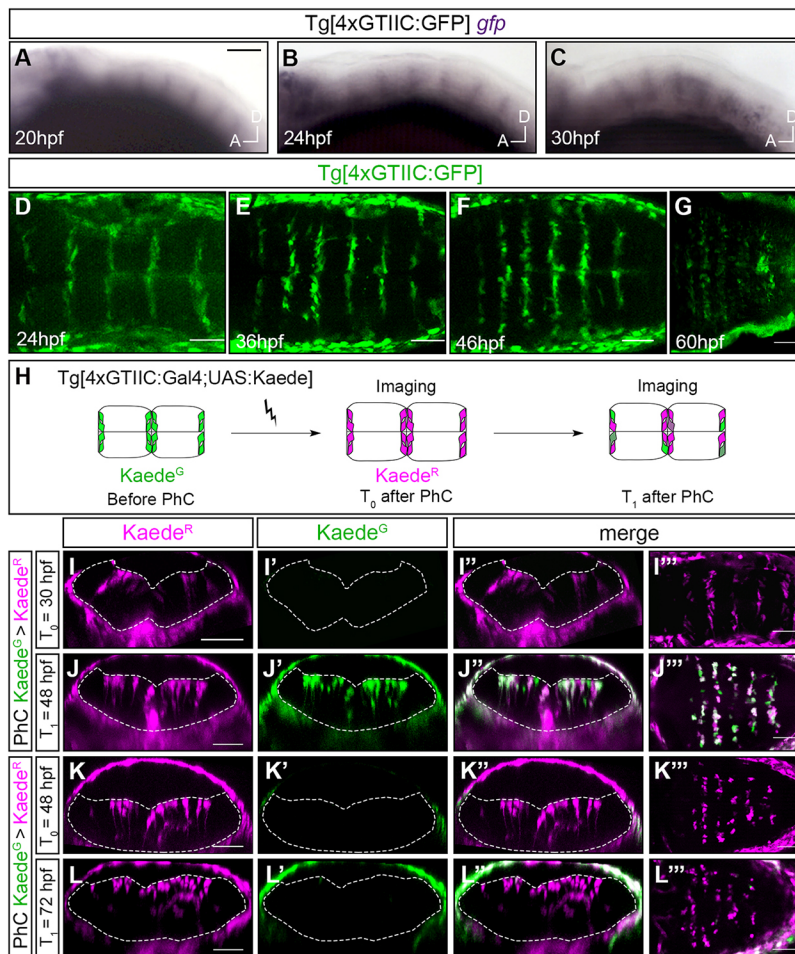


**Fig. 2. Onset/offset of Yap/Taz-TEAD activity in the hindbrain boundaries.** (A-C) Tg[4xGTIIC:GFP] embryos at the indicated stages assayed for a whole-mount *in situ* hybridization using a *gfp* RNA probe. Expression of *gfp*, and therefore Yap/Taz-activity, is already visible in the boundaries at 20 hpf. Lateral views with anterior to the left. (D-G) Expression of GFP in the hindbrain boundaries in Tg[4xGTIIC:GFP] embryos at the indicated stages. GFP is first observed at 25 hpf. GFP expression persists for up to 72 hpf (data not shown). Dorsal views with anterior to the left. (H) Scheme depicting the photoconversion experiment: Kaede<sup>G</sup> in the hindbrain boundary cells of Tg[4xGTIIC:Gal4;UAS:KAED] embryos was photoconverted to Kaede<sup>R</sup> at T<sub>0</sub>, and embryos were allowed to develop up to the desired stage (T<sub>1</sub>). (I-I'', J-J'') Embryo in which Kaede<sup>G</sup> was photoconverted to Kaede<sup>R</sup> at T<sub>0</sub>=30 hpf (I-I'') and which was analyzed at T<sub>1</sub>=48 hpf (J-J''). New Kaede<sup>G</sup> is generated in cells between 30 hpf and 48 hpf (see merged channels in J'', J''). (K-K'') Embryo in which Kaede<sup>G</sup> was photoconverted to Kaede<sup>R</sup> at T<sub>0</sub>=48 hpf (K-K'') and which was further analyzed at T<sub>1</sub>=72 hpf (L-L''). No new Kaede<sup>G</sup>-expressing cells were observed after photoconversion (L-L''), suggesting that the decline of Yap/Taz-activity was before 48 hpf. (I-I'', J-J'', K-K'', L-L'') Reconstructed transverse sections of embryos are displayed in I'', J'', K'', L'' as dorsal views with anterior to the left. Scale bars: 30 μm in A-C; 50 μm in D-G, I-L''.

(Letelier et al., 2018), using MO-Rac3b (Fig. 3H,  $n=31/38$  embryos that lost *gfp* expression in boundary cells), whereas embryos injected with a random morpholino did not display this phenotype (Fig. 3G,  $n=4/22$  with no *gfp* expression). In all cases, this downregulation was not evenly affecting the whole TEAD activity in the embryo, as Yap/Taz-TEAD activity within the somites, for example, was maintained (Fig. 3B,C,H). Pharmacological treatments did not interfere with boundary cell identity, as expression of *rfig* was not affected (Fig. 3D-F), did not delay hindbrain development or alter rhombomere morphology (Gutzman and Sive, 2010), and did not affect the interkinetic nuclear migration ratio or the number of mitotic cells (Calzolari et al., 2014). Complementary results were obtained following conditional downregulation of Rac3b and posterior clonal analysis (Fig. 3I-K). In these experiments, Tg[4xGTIIC:GFP] embryos were injected with either hsp:Myc or Myc:hsp:Rac3bDN constructs, heat-shocked and allowed to develop until 30 hpf, when the percentage of green GFP-positive (Yap/Taz-activity) and magenta Myc-expressing (Myc or Myc:Rac3bDN) clones within the boundaries was analyzed (Fig. 3J-K). In the control hsp:Myc-injected embryos, the majority of boundary clones expressing Myc displayed Yap/Taz activity (Fig. 3K, 95%  $n=20/21$ ). In contrast, the majority of boundary clones in the Myc:Rac3bDN-injected embryos that expressed Myc (and therefore Rac3bDN) did not express Yap/Taz-activity (see Fig. 3J-J'' as an example; Fig. 3K, 70%,  $n=33/47$ ). Thus, boundary cells responded to mechanical cues in a cell-autonomous manner through Yap/Taz-TEAD activity. To further demonstrate that Yap and Taz were instrumental for TEAD activity within the boundary cells, we disrupted the actomyosin cables in

Tg[4xGTIIC:GFP] embryos and assessed the expression of Yap and Taz proteins in the boundaries (Fig. 3L-O). Indeed, treatment with blebbistatin resulted in a loss of Yap expression in the hindbrain boundaries (Fig. 3M; blebbistatin,  $n=10/12$  embryos with loss of Yap expression in the boundary cells) when compared with DMSO treatment (Fig. 3L; DMSO,  $n=3/24$  embryos with no Yap boundary expression). Similar results were obtained when the expression of Taz was analyzed (Fig. 3N,O; DMSO,  $n=1/30$  versus blebbistatin,  $n=12/14$  embryos displaying loss of Taz expression in boundaries). As expected, blebbistatin-treated embryos did not display Yap/Taz-TEAD activity (Fig. 3M',  $n=12/12$ ; Fig. 3O',  $n=13/14$  with no TEAD-activity in the boundaries) when compared with control embryos (Fig. 3L',  $n=26/30$ ; Fig. 3N',  $n=20/30$  embryos expressing GFP in the boundaries).

### Yap/Taz-TEAD active boundary cells switch the proliferative behavior over time

We next studied the spatiotemporal dynamics of Yap/Taz-TEAD active cells by exploring their lineage. For this purpose, we established a 4D-imaging pipeline that allowed us to reconstruct cell lineage trees and analyze cell behavior (Movie 1, Fig. 4A). We took advantage of the high temporal coverage and resolution provided by single plane illumination microscopy over multiple embryos encompassing the onset and offset of Yap/Taz-activity (Table 1, Fig. S2). Tg[4xGTIIC:GFP] embryos were injected either at the one-cell stage with hsp:H2B-RFP and heat-shocked at 26 hpf, or at the eight-cell stage with *H2B-mCherry*, and imaged as indicated in Fig. 4A and Fig. S2. The lineage of 63 single GFP-positive cells

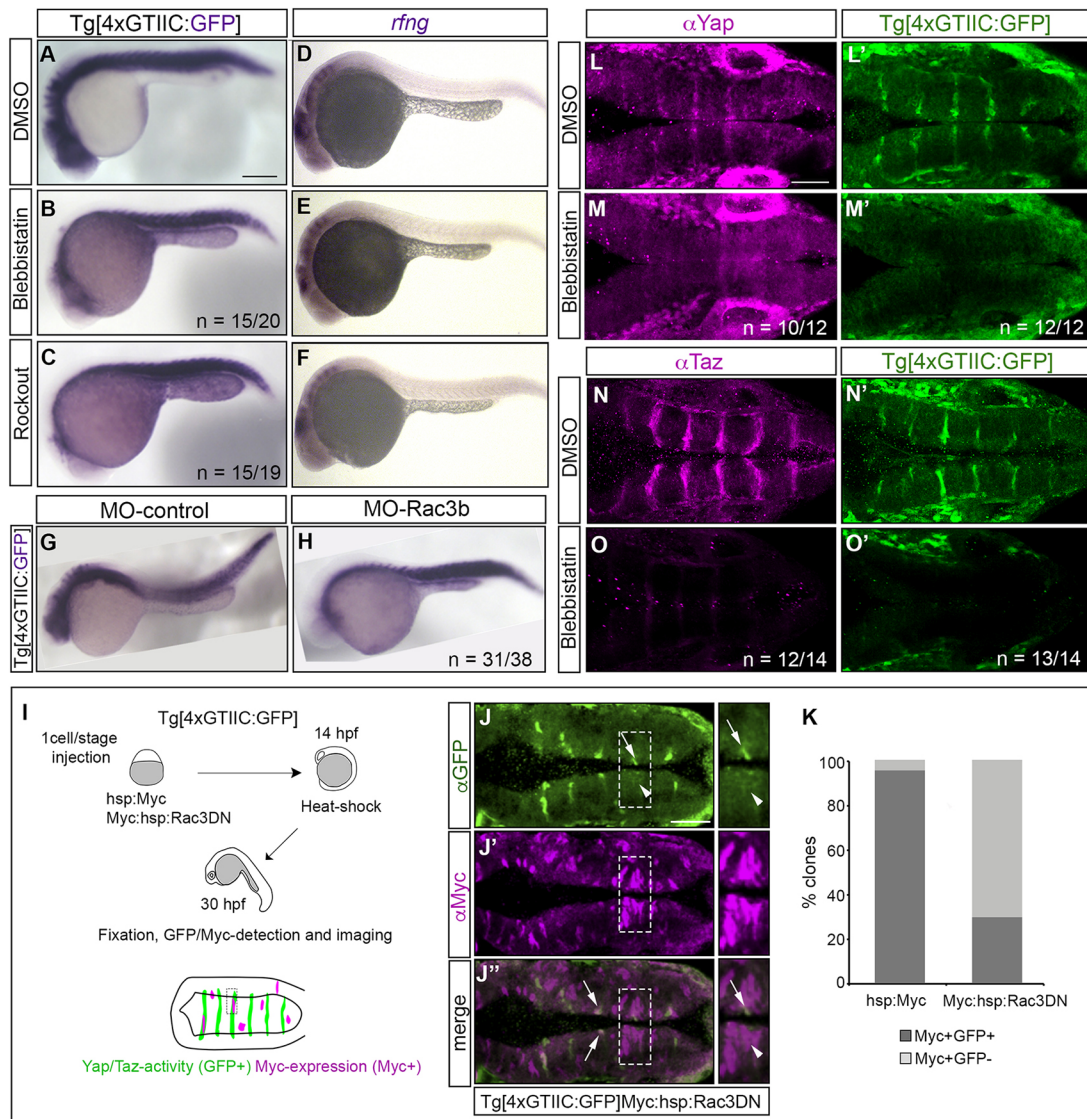


**Fig. 3. Yap and Taz in the hindbrain boundaries sense mechanical cues.** (A-C, G, H) Whole-mount *gfp in situ* hybridization of Tg[4xGTIIC:GFP] embryos treated with DMSO (A), with myosin II pharmacological inhibitors such as blebbistatin (B) and rockout (C) from 16 to 22 hpf, or injected with MO-control (G) or MO-Rac3b (H) in order to downregulate Rac3b. In all distinct experimental cases, *gfp* expression, and therefore Yap/Taz activity, is downregulated in the hindbrain boundaries and is not affected in the somites. (D-F) Whole-mount *rng in situ* hybridization of Tg[4xGTIIC:GFP] embryos treated with DMSO (D), blebbistatin (E) or rockout (F). Expression of boundary markers is not affected upon treatment, as previously shown (Gutzman and Sive, 2010). Lateral views with anterior to the left. (I-K) Downregulation of Rac3b by clonal analysis. (I) Scheme depicting the functional experiment in which Tg[4xGTIIC:GFP] embryos were injected at the one-cell stage with inducible Myc-tagged constructs (hsp:Myc or Myc:hsp:Rac3DN), heat-shocked at 14 hpf, allowed to develop until 30 hpf, and immunostained for GFP and Myc. For the phenotypic analysis, we scored the percentage of Myc-expressing clones (Myc-positive) hitting the boundaries that displayed Yap/Taz-TEAD activity (GFP-positive) and this was plotted in K. (J-J'') Example of a Tg[4xGTIIC:GFP] embryo injected with Myc:hsp:Rac3DN and immunostained using anti-GFP (green) and anti-Myc (magenta) antibodies. Myc-positive cells, when located within the boundaries, display low (see arrows) or no (see arrowheads) GFP-expression. On the right are images from the regions framed in J-J'' showing a magnified boundary in which the Yap/Taz-TEAD activity has been either completely abolished or downregulated upon expression of Rac3DN. Dorsal view with anterior to the left. (K) The percentage of boundary cell clones expressing Yap/Taz-TEAD activity (GFP-positive clones) are displayed in dark gray in the histogram, over the total Myc-positive clones displayed as light gray in the histogram, either in control (hsp:Myc) or experimental conditions (Myc:hsp:Rac3DN) where the actomyosin cables were compromised. When Rac3b is downregulated, the percentage of Myc-positive clones with Yap/Taz-TEAD activity decreases. (L-O') Tg[4xGTIIC:GFP] embryos treated with DMSO (L, L', N, N') or with blebbistatin (M, M', O, O') from 19-25 hpf, and immunostained using anti-Yap (L, M) or anti-Taz (N, O) antibodies, and analyzed for TEAD activity (L', M', N', O'). Expression of GFP and Yap and Taz in the boundary cells is abolished upon blebbistatin treatment. Dorsal views with anterior to the left. r, rhombomere. n=X/Y indicates the number of embryos with the displayed phenotype (X) over the total number of analyzed embryos (Y). Scale bars: 200 $\mu$ m in A-H; 50 $\mu$ m in J-J'', L-O.

expressing RFP/mCherry in the nucleus was reconstructed over an average of 20 h of imaging (see Movie 1 for an example of a single cell tracking), and cell behavior was assessed according to: (1) cell division (dividing/non-dividing; Fig. 4B-E); and (2) cell differentiation (progenitor/differentiated; Fig. 4F-J'') status. For the analysis of cell proliferation, cells were plotted as a lineage tree in

which each line indicated a single cell (Fig. 4B). Most of the cells that were tracked from 26 hpf onwards actively proliferated and are individually depicted as single lines branching upon cell division (orange lines in Fig. 4B). Movie 1 and Fig. 4C, C' showed a cell undergoing two divisions and giving rise to four daughter cells. However, from 40 hpf onwards, the cells displayed a clear switch in

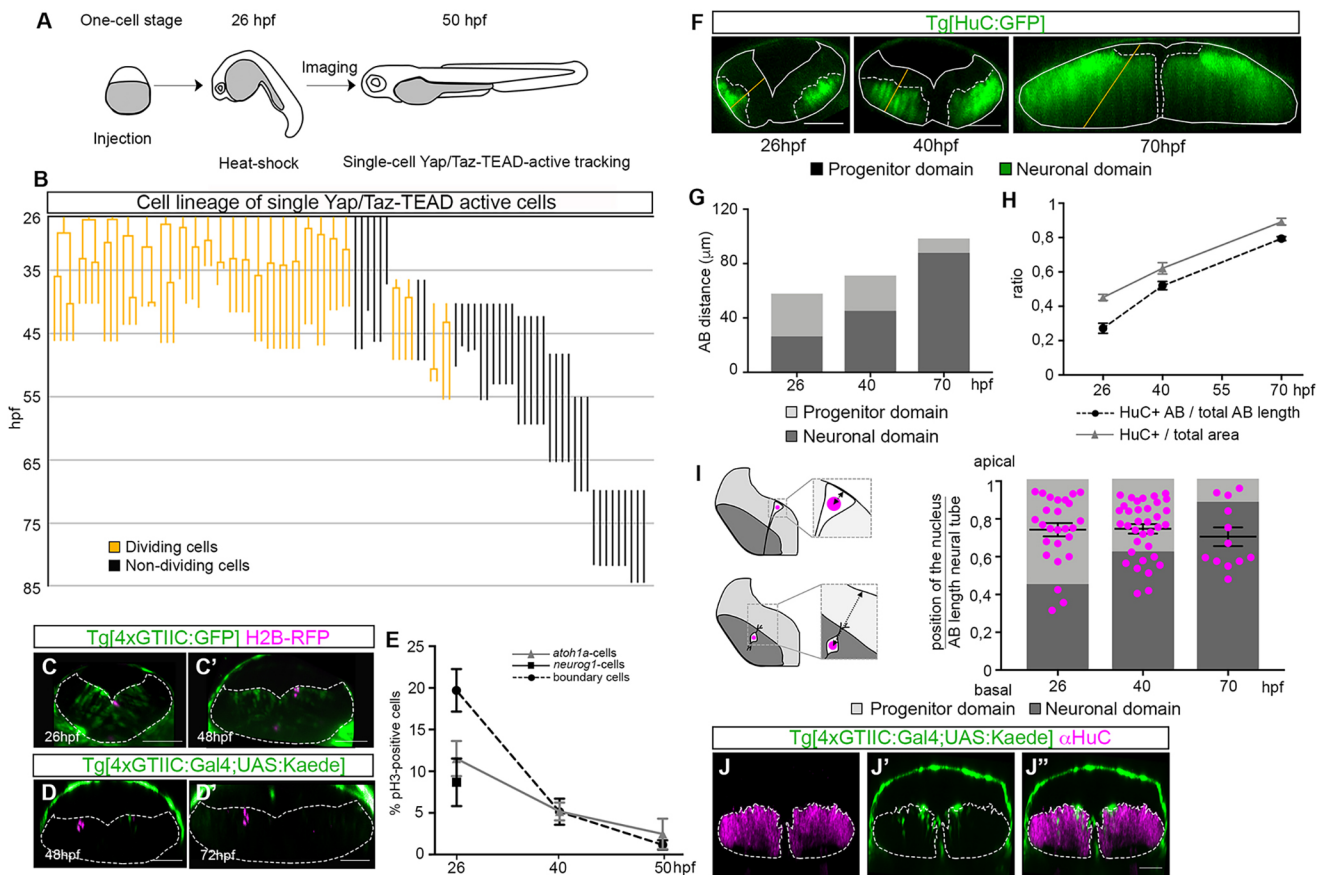


**Fig. 4. Boundary cells switch their proliferative behavior over time.** (A) Scheme depicting the outline of the experiment: Tg[4xGTIIC:GFP] embryos were injected at the one-cell stage with hsp:H2B-RFP and heat-shocked at 26 hpf, or were injected at the eight-cell stage with *H2B-mCherry* (not shown). Embryos displaying red nuclei within the Yap/Taz-active boundary cells were then imaged up to the desired stage (Fig. S2). (B) Representation of the Yap/Taz-TEAD active cell lineage tree with the y-axis displaying the time of embryonic development in hours post-fertilization (hpf). The 63 cell lineages are displayed from the moment of tracking onwards and are color-coded according to proliferative behavior (orange, dividing; black, non-dividing). Each line corresponds to a single cell tracked starting from the beginning of the movie until the end (Table 1); branches indicate cell divisions. An interrupted line means either the end of the movie or that the cell was lost from the field. There is a switch in cell proliferative behavior from 40 hpf onwards, from which time most of the 4xGTIIC:GFP cells do not divide and therefore do not branch. Yap/Taz-active derivatives can be tracked beyond Yap/Taz-TEAD activity due to the stability of the GFP protein. (C,C') Stills from a time-lapse movie that followed a single cell from 26 hpf to 48 hpf; the cell underwent two cell divisions giving rise to four cells (Movie 1). (D,D') Representative example of a group of three cells photoconverted at 48 hpf and followed until 72 hpf. The number of cells does not change during this 24 h period, supporting the previous observation of a switch in cell proliferation behavior. (E) Graph showing the percentage of cells undergoing cell division over time in different hindbrain cell populations: Yap/Taz-TEAD proliferating boundary cells (black circles and dashed line); *atoh1a*-positive rhombomeric cells (gray triangles and solid line) and *neurog1*-positive cells (black square) in the flanking boundary regions. There is a difference in the percentage of cells undergoing mitosis in boundaries (19%) versus other hindbrain territories (*atoh1a*-positive cells, 11.5%; *neurog1*-positive cells, 8.5%) at 26 hpf; the boundary cell population dramatically changes its proliferative behavior after the offset of Yap/Taz-activity (5.7% at 40 hpf). (F) Images showing the development of the neuronal differentiation domain in Tg[HuC:GFP] embryos from 26 hpf to 70 hpf. (G) Histogram displaying the actual size of the progenitor versus neuronal domains at the indicated stages. Data were obtained from Tg[HuC:GFP] embryos whose apicobasal (AB) length was measured (the length extending from the apical ventricular zone edge to the basal mantle zone according to cell orientation within the neural epithelium;  $n=8-10$  boundaries of four or five embryos/stage). There is a dramatic increase in the size of the neuronal domain at the expense of the progenitor domain over time. (H) Comparison of the two methods used for growth assessment. The ratio of distances measured between the apical/ventricular and basal/mantle borders of the HuC domain (black circles and dashed line) versus the measurement of the HuC area (gray triangles and solid line) of an average of 12-18 boundaries (6-9 embryos) is shown. These two approaches provide equivalent estimates of progenitor/neuronal domain progression. (I) Analysis of the position along the apicobasal axis of the nuclei of cells tracked in B at different times. Positional values were plotted (magenta dots) and overlaid with the information obtained from the progenitor/neuronal map. Briefly, nuclear position was scored by measuring the distance from the cell nucleus to the apical side, according to the drawing, and the result was normalized taking into consideration the thickness of the neural tube (see Materials and Methods). Most of the cell nuclei lay within the progenitor domain (light-gray zone) at 26 hpf, whereas at 70 hpf they were mainly located in the neuronal differentiated domain (dark-gray zone). (J-J'') Immunostaining of Tg[4xGTIIC:Gal4;UAS:KAEDE] embryos using anti-HuC antibodies at 50 hpf, showing derivatives of Yap/Taz-active cells within the HuC-positive domain. Although cells within the neuronal domain are not active for Yap/Taz (as shown in Fig. 2), their derivatives can be tracked due to the stability of the KAEDE protein. Scale bars: 50  $\mu$ m.

their proliferative behavior and after this time most of the tracked cells did not divide any further (black lines in Fig. 4B). Although at late stages cells did not express *de novo* GFP because no new activity was triggered (Fig. 2), the derivatives of these cells could be tracked due to the stability of the GFP protein. The change in cell proliferative behavior could also be observed when three KAEDE<sup>G</sup>-

cells were photoconverted at 48 hpf, following which the number of KAEDE<sup>R</sup>-cells remained unchanged 24 h later (Fig. 4D,D'). Interestingly, a similar behavioral switch was observed when cell proliferation was assessed using an alternative approach such as quantification of mitotic figures (Fig. 4E). Such quantification showed that the number of Yap/Taz-TEAD active boundary cells

**Table 1. Cohort of embryos and datasets**

| ID dataset | Transgenic embryo | DNA injection | Timestep imaging | Imaging sequences |
|------------|-------------------|---------------|------------------|-------------------|
| 170117     | Tg[4xGTIIC:d2GFP] | hsp:H2B-RFP   | 6 min            | 36–49 hpf         |
| 170118     | Tg[4xGTIIC:d2GFP] | hsp:H2B-RFP   | 6 min            | 40–53 hpf         |
| 170119     | Tg[4xGTIIC:d2GFP] | hsp:H2B-RFP   | 6 min            | 48–65.5 hpf       |
| 170125     | Tg[4xGTIIC:d2GFP] | H2B-mCherry   | 6 min            | 40–55.5 hpf       |
| 170127     | Tg[4xGTIIC:d2GFP] | H2B-mCherry   | 7 min            | 42–59.5 hpf       |
| 170128     | Tg[4xGTIIC:d2GFP] | H2B-mCherry   | 7 min            | 70–85 hpf         |
| 170206     | Tg[4xGTIIC:d2GFP] | H2B-mCherry   | 7 min            | 40–54 hpf         |
| 170207     | Tg[4xGTIIC:d2GFP] | H2B-mCherry   | 7 min            | 55–69 hpf         |
| 170208     | Tg[4xGTIIC:d2GFP] | H2B-mCherry   | 7 min            | 70–86.2 hpf       |
| 170215     | Tg[4xGTIIC:d2GFP] | hsp:H2B-RFP   | 7 min            | 26–41 hpf         |
| 170216     | Tg[4xGTIIC:d2GFP] | hsp:H2B-RFP   | 7 min            | 26–41 hpf         |
| 170222     | Tg[4xGTIIC:d2GFP] | hsp:H2B-RFP   | 7 min            | 26–41 hpf         |
| 170223     | Tg[4xGTIIC:d2GFP] | hsp:H2B-RFP   | 7 min            | 26–41.4 hpf       |
| 170301a    | Tg[4xGTIIC:d2GFP] | hsp:H2B-RFP   | 7 min            | 26–47 hpf         |
| 170301b    | Tg[4xGTIIC:d2GFP] | hsp:H2B-RFP   | 7 min            | 26–47.2 hpf       |
| 171108     | Tg[4xGTIIC:d2GFP] | hsp:H2B-RFP   | 7 min            | 26–41 hpf         |
| 171109     | Tg[4xGTIIC:d2GFP] | hsp:H2B-RFP   | 7 min            | 26–41 hpf         |

Datasets used in this study with corresponding information regarding transgenic embryos and cDNA injections used for Fig. 4 experiments. The temporal frequency of image acquisition (timestep imaging) and corresponding imaging sequences are indicated.

undergoing mitosis dramatically decreased from 26 hpf to 50 hpf ( $19.5 \pm 2.3\%$  at 26 hpf versus  $5.7 \pm 1.4\%$  at 40 hpf versus  $2.1 \pm 0.5\%$  at 50 hpf). On the other hand, adjacent non-boundary cells displayed a different proliferative behavior: the percentage of proliferating *neurog1*- and *atoh1a*-positive cells at 26 hpf was half that of the boundary cells (Fig. 4E; *neurog1*-cells,  $8.5 \pm 2.6\%$ ; *atoh1a*-cells,  $11.5 \pm 1.9\%$ , compared with  $19.5 \pm 2.3\%$  of boundary cells), with a smaller decrease over time (*atoh1a*-cells,  $5.9 \pm 0.9\%$  at 40 hpf;  $3.2 \pm 1.6\%$  at 50 hpf; Fig. 4E). In summary, the reconstruction of the lineage of Yap/Taz-active boundary cells from *in vivo* data demonstrate that these cells display not only a different proliferative activity compared with their neighbors at 26 hpf, but that they undergo a proliferation switch around 40 hpf that coincides with the temporal window in which Yap/Taz-TEAD activity decreases.

To determine whether this switch in the proliferative behavior of boundary cells was related to the cell differentiation status (progenitor versus differentiated neuron), we assessed the fate of these tracked Yap/Taz-TEAD cells by tracing their spatial distribution (position in the ventricular versus mantle domains) over time. To achieve this, we first generated a dynamic map of differentiated neurons within the hindbrain boundary region (Fig. 4F) by comparing the growth of the differentiation domain (HuC-positive territory) versus the progenitor domain (HuC-negative territory). A large expansion of the differentiation domain was observed from 26 hpf to 70 hpf (Fig. 4F,G), which required a decrease in the progenitor domain (Fig. 4G). The use of the apicobasal (AB) distances for growth assessment was equivalent to the use of HuC areas, as depicted in Fig. 4H. We then plotted the position of the nuclei along the AB axis of the previously tracked cells on the top of the progenitor/differentiation map (Fig. 4I). Cell nuclei position was assessed by measuring the distance of each cell nucleus to the ventricular zone at different time steps of the movie (see scheme in Fig. 4I). This feature was used as a readout of the cell differentiation state: nuclei located close to the apical side correspond to progenitor cells (light gray, Fig. 4I), whereas nuclei close to the basal side correspond to differentiated neurons (dark gray, Fig. 4I). At the onset of Yap/Taz-TEAD activity, most of the nuclei of tracked cells were found in the progenitor domain (see magenta dots on the light gray histogram at 26 hpf in Fig. 4I). Later on, most of the Yap/Taz-derivatives were found within the differentiation domain (neuronal domain; see magenta dots on the dark-gray histogram at 40 and 70 hpf in Fig. 4I).

This switch in nuclei position of the tracked cells coincided with the previously observed change in proliferative activity, suggesting that Yap/Taz-active cells within the boundaries behaved as progenitors until they switched off Yap/Taz-TEAD activity. They then ceased proliferating and underwent neuronal differentiation. Most probably boundaries need to balance the ratio of progenitors versus differentiated neurons as is done in other parts of the neural tube (Hiscock et al., 2018). The fact that we observed Yap/Taz-TEAD derivatives in the neuronal differentiation domain was due to the high stability of KAEDE (see green cells within the magenta territory Fig. 4J–J’).

#### Yap/Taz-activity regulates progenitor cell behavior in the hindbrain boundaries

To investigate whether Yap and Taz were indeed regulating the proliferative behavior of boundary cells, we knocked-down *yap* or *taz* (*wwtr1*) and compared the effects of their downregulation on cell apoptosis and proliferative activity between boundary cells (Fig. 5A,B,E,F) and non-boundary cells (Fig. 5C,D,G,H). First, to dissect the contribution of Yap and Taz in these activities, we followed the TEAD activity in Tg[4xGTIIC:GFP] embryos in which either Yap or Taz was downregulated by a splice- or a translation-blocking morpholino (Fig. S3A–F). No changes in TEAD activity were observed upon downregulation of either co-factor alone, suggesting that Yap and Taz function redundantly within the boundary cell population (Fig. S3G–I). To further test this possibility, we knocked-down *yap* in a *taz* (*wwtr1*) mutant (*wwtr1<sup>fu55</sup>*; Fig. S3J,L). Downregulation of Yap in the *wwtr1<sup>fu55/+</sup>* mutant background had no effect on the number of apoptotic cells, either in the boundaries (Fig. 5A; Table 2) or in the rhombomeric cells (Fig. 5C; Table 3). However, it did result in a decrease in the number of proliferating boundary cells (Fig. 5B; Table 2), but not in that of the rhombomeric cells (Fig. 5D; Table 3). We used *wwtr1* heterozygous mutants (*wwtr1<sup>fu55/+</sup>*) injected with MO-Yap for these experiments, because injection of MO-Yap into *wwtr1<sup>fu55</sup>* homozygous mutant embryos led to early mortality. The obtained results suggested that Yap/Taz-activity specifically regulated the proliferation of hindbrain boundary cells.

To confirm this possibility, we performed the same analysis by using a combination of *yap/wwtr1* compound mutants (Fig. S3J–L). No changes in cell apoptosis within the hindbrain were observed

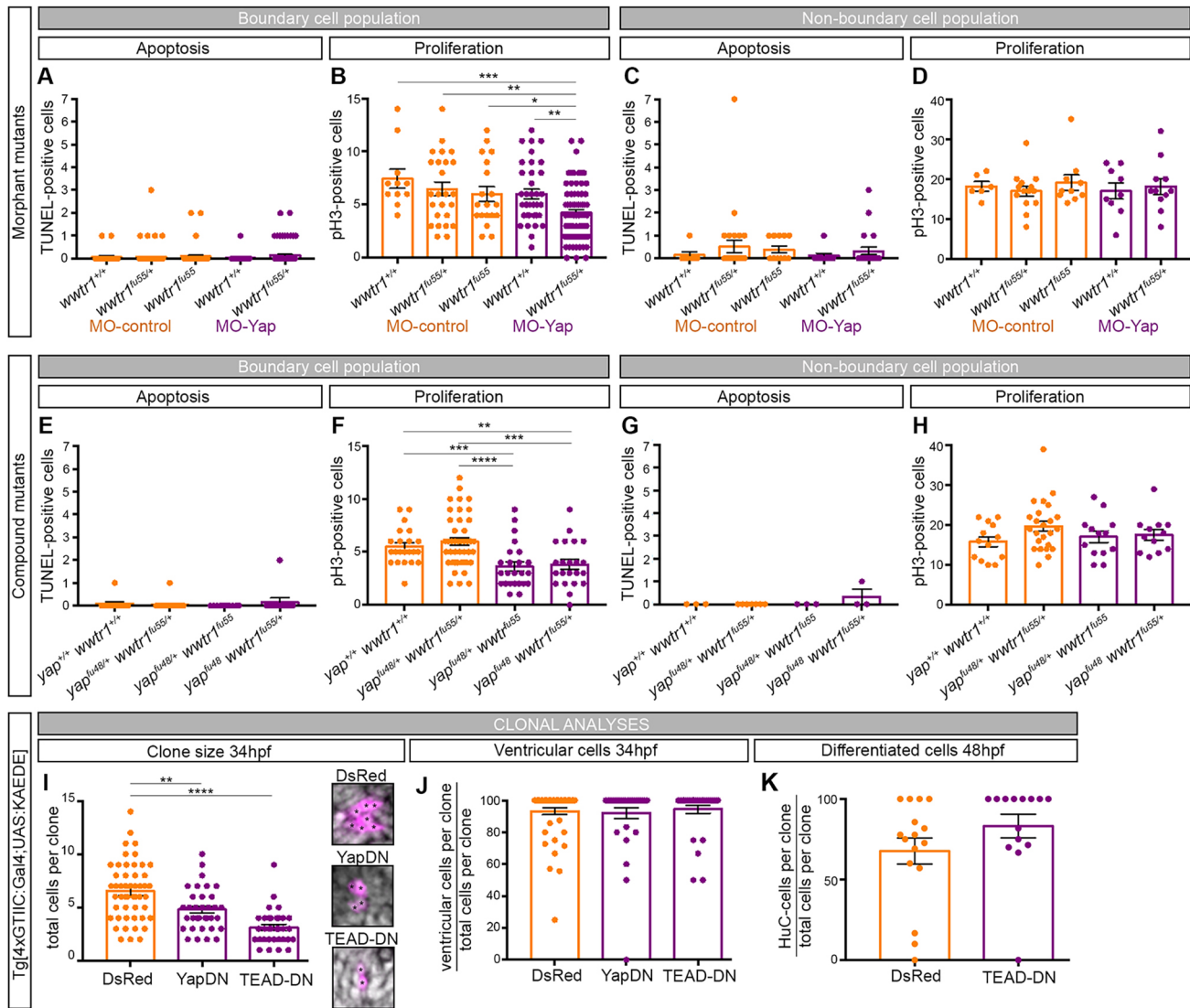


**Fig. 5. Yap/Taz-activity regulates the proliferative behavior of hindbrain boundary cells.** (A–D) Wild-type (*wwtr1*<sup>+/+</sup>), heterozygous (*wwtr1*<sup>fu55/+</sup>) or homozygous (*wwtr1*<sup>fu55/fu55</sup>) embryos for *taz* mutation were injected with MO-control, and wild-type (*wwtr1*<sup>+/+</sup>) or heterozygous (*wwtr1*<sup>fu55/+</sup>) embryos were injected with MO-Yap, and the number of apoptotic (A,C) and proliferating (B,D) cells within the hindbrain boundaries (A,B; Table 2) or in the non-boundary region of r5 (C, D; Table 3) was quantified at 34 hpf. We used the borders of *epha4* expression in r3 (r2/r3, r3/r4) and r5 (r4/r5, r5/r6) as boundary landmarks, and *epha4* expression in r5 for non-boundary regions (see Materials and Methods). Each dot corresponds to the number of scored cells in a single boundary/rhombomere. *P* values for B are: MO-control *wwtr1*<sup>+/+</sup> versus MO-Yap *wwtr1*<sup>fu55/+</sup>, \*\*\**P*=0.0008; MO-control *wwtr1*<sup>fu55/+</sup> versus MO-Yap *wwtr1*<sup>fu55/+</sup>, \*\**P*=0.0026; MO-control *wwtr1*<sup>fu55/fu55</sup> versus MO-Yap *wwtr1*<sup>+/+</sup>, \**P*=0.0361; MO-Yap *wwtr1*<sup>+/+</sup> versus MO-Yap *wwtr1*<sup>fu55/+</sup>, \*\**P*=0.0027. (E,F) Wild-type (*yap*<sup>+/+</sup>*wwtr1*<sup>+/+</sup>), double heterozygous (*yap*<sup>fu48/+</sup>*wwtr1*<sup>fu55/+</sup>) or compound mutant (*yap*<sup>fu48/+</sup>*wwtr1*<sup>fu55/fu55</sup>, *yap*<sup>fu48/+</sup>*wwtr1*<sup>fu55/+</sup>) embryos for *yap* and *wwtr1* were used to assess the number of apoptotic (E,G) and proliferating cells (F,H) within the hindbrain boundaries (E,F; Table 2) or in the non-boundary region of r5 (G,H; Table 3). *P* values for F are: *yap*<sup>+/+</sup>*wwtr1*<sup>+/+</sup> versus *yap*<sup>fu48/+</sup>*wwtr1*<sup>fu55/fu55</sup>, \*\*\**P*=0.0006; *yap*<sup>+/+</sup>*wwtr1*<sup>+/+</sup> versus *yap*<sup>fu48/+</sup>*wwtr1*<sup>fu55/+</sup>, \*\**P*=0.0042; *yap*<sup>fu48/+</sup>*wwtr1*<sup>fu55/+</sup> versus *yap*<sup>fu48/+</sup>*wwtr1*<sup>fu55/fu55</sup>, \*\*\*\**P*<0.0001; *yap*<sup>fu48/+</sup>*wwtr1*<sup>fu55/+</sup> versus *yap*<sup>fu48/+</sup>*wwtr1*<sup>fu55/fu55</sup>, \*\*\**P*=0.0006. Tables 2 and 3 provide the numbers of embryos used for each genotype analysis. Upon downregulation of Yap in *wwtr1* mutants, or when at least three of the *yap/wwtr1* alleles were mutated, the number of dividing cells decreased within the boundaries. (I,J) Tg[4xGTIIIC:Gal4;UAS:KAEDE] embryos were injected with UAS:DsRed (DsRed), UAS:DsRed-YapDN (YapDN) or UAS:DsRed-TEAD-DN (TEAD-DN) forms to genetically and conditionally induce clones expressing DsRed constructs only in the Yap/Taz-active cells. Embryos with cell clones were analyzed and the clone size was assessed by the number of cells displaying DsRed in each clone (I). Photomicrographs show examples of clones obtained upon different construct injections (cells colored in magenta) and the asterisks indicate single cells within the clone. The number of cells in DsRed clones is higher than in YapDN or TEAD-DN clones. The position of the clone along the apicobasal axis was determined at 34 hpf by measuring the number of ventricular cells per clone over the total number of cells in the clone (J). The effects of triggering neuronal differentiation were analyzed at 48 hpf (K). Clones in which Yap/Taz-TEAD was downregulated have fewer cells than the control clones. However, no differences were observed in the differentiation rate. *P* values for I are: UAS:DsRed versus UAS:DsRed-YapDN, \**P*=0.0021; UAS:DsRed versus UAS:DsRed-TEAD-DN, \*\*\*\**P*<0.0001. \**P*≤0.05, \*\**P*≤0.01, \*\*\**P*≤0.001, \*\*\*\**P*≤0.0001. The non-parametric Mann–Whitney test was used.

(Fig. 5E,G; Table 2); however, the number of boundary cells undergoing mitosis was lower in all *yap/wwtr1* compound mutants, with three mutated alleles (*yap*<sup>fu48/+</sup>*wwtr1*<sup>fu55</sup> and *yap*<sup>fu48/+</sup>*wwtr1*<sup>fu55/+</sup>) when compared with the number in the other analyzed genotypes

(Fig. 5F; Table 2). Again, no defects were observed in any of the mutant combinations when non-boundary regions were analyzed (Fig. 5H; Table 3). The regulation of the proliferative capacity within the boundary cells in these mutants was mainly due to the loss of



**Table 2. Embryos used for functional analysis in the hindbrain boundaries**

| Figure  | Genotype  | Number of boundaries | Number of embryos |
|---------|---|----------------------|-------------------|
| Fig. 5A | MO-control <i>wwtr1</i> <sup>+/+</sup>                      | 28                   | 7                 |
|         | MO-control <i>wwtr1</i> <sup>fu55/+</sup>                   | 108                  | 27                |
|         | MO-control <i>wwtr1</i> <sup>fu55</sup>                     | 52                   | 13                |
|         | MO-Yap <i>wwtr1</i> <sup>+/+</sup>                          | 36                   | 9                 |
|         | MO-Yap <i>wwtr1</i> <sup>fu55/+</sup>                       | 88                   | 22                |
| Fig. 5B | MO-control <i>wwtr1</i> <sup>+/+</sup>                      | 11                   | 7                 |
|         | MO-control <i>wwtr1</i> <sup>fu55/+</sup>                   | 25                   | 13                |
|         | MO-control <i>wwtr1</i> <sup>fu55</sup>                     | 19                   | 10                |
|         | MO-Yap <i>wwtr1</i> <sup>+/+</sup>                          | 37                   | 19                |
|         | MO-Yap <i>wwtr1</i> <sup>fu55/+</sup>                       | 73                   | 37                |
| Fig. 5E | <i>yap</i> <sup>+/+</sup> <i>wwtr1</i> <sup>+/+</sup>       | 12                   | 3                 |
|         | <i>yap</i> <sup>fu48/+</sup> <i>wwtr1</i> <sup>fu55/+</sup> | 28                   | 7                 |
|         | <i>yap</i> <sup>fu48/+</sup> <i>wwtr1</i> <sup>fu55</sup>   | 12                   | 3                 |
|         | <i>yap</i> <sup>fu48</sup> <i>wwtr1</i> <sup>fu55/+</sup>   | 12                   | 3                 |
|         | <i>yap</i> <sup>+/+</sup> <i>wwtr1</i> <sup>+/+</sup>       | 22                   | 15                |
| Fig. 5F | <i>yap</i> <sup>fu48/+</sup> <i>wwtr1</i> <sup>fu55/+</sup> | 45                   | 36                |
|         | <i>yap</i> <sup>fu48/+</sup> <i>wwtr1</i> <sup>fu55</sup>   | 23                   | 15                |
|         | <i>yap</i> <sup>fu48</sup> <i>wwtr1</i> <sup>fu55/+</sup>   | 22                   | 17                |
|         |   |                      |                   |

Numbers indicate the number of embryos used for the analysis and the number of boundaries analyzed for Fig. 5.

TEAD activity, as *yap/wwtr1* compound mutants with three mutated alleles did not display TEAD activity within these cells (Fig. S3M,N; *yap*<sup>fu48/+</sup> *wwtr1*<sup>fu55</sup> *n*=12/14).

Finally, to avoid the deleterious effects of the mutations and to determine whether the observed effect was cell-autonomous, we conditionally decreased Yap/Taz activity within the TEAD-active cells by injection of dominant-negative forms of Yap and TEAD (UAS:DsRed-YapDN, UAS:DsRed-TEAD-DN; Miesfeld et al., 2015) into Tg[4xGTTC:Gal4;UAS:KAEDE] embryos. Clones expressing DsRed constructs were evaluated for cell size and position at 34 hpf and 48 hpf, respectively. In all cases in which TEAD activity was downregulated, either by Yap-DN or TEAD-DN, we observed a decrease in the number of cells per clone (Fig. 5I; UAS:DsRed-YapDN=4.78±0.34 cells/clone; UAS:DsRed-TEAD-DN=3.12±0.29 cells/clone) when compared with control UAS:DsRed-injected embryos (Fig. 5I; 6.54±0.38 cells/clone).

**Table 3. Embryos used for functional analysis in the rhombomeres**

| Figure  | Genotype  | Number of embryos |
|---------|---|-------------------|
| Fig. 5C | MO-control <i>wwtr1</i> <sup>+/+</sup>                      | 7                 |
|         | MO-control <i>wwtr1</i> <sup>fu55/+</sup>                   | 27                |
|         | MO-control <i>wwtr1</i> <sup>fu55</sup>                     | 13                |
|         | MO-Yap <i>wwtr1</i> <sup>+/+</sup>                          | 9                 |
|         | MO-Yap <i>wwtr1</i> <sup>fu55/+</sup>                       | 22                |
| Fig. 5D | MO-control <i>wwtr1</i> <sup>+/+</sup>                      | 6                 |
|         | MO-control <i>wwtr1</i> <sup>fu55/+</sup>                   | 14                |
|         | MO-control <i>wwtr1</i> <sup>fu55</sup>                     | 10                |
|         | MO-Yap <i>wwtr1</i> <sup>+/+</sup>                          | 10                |
|         | MO-Yap <i>wwtr1</i> <sup>fu55/+</sup>                       | 11                |
| Fig. 5G | <i>yap</i> <sup>+/+</sup> <i>wwtr1</i> <sup>+/+</sup>       | 3                 |
|         | <i>yap</i> <sup>fu48/+</sup> <i>wwtr1</i> <sup>fu55/+</sup> | 7                 |
|         | <i>yap</i> <sup>fu48/+</sup> <i>wwtr1</i> <sup>fu55</sup>   | 3                 |
|         | <i>yap</i> <sup>fu48</sup> <i>wwtr1</i> <sup>fu55/+</sup>   | 3                 |
|         | <i>yap</i> <sup>+/+</sup> <i>wwtr1</i> <sup>+/+</sup>       | 13                |
| Fig. 5H | <i>yap</i> <sup>fu48/+</sup> <i>wwtr1</i> <sup>fu55/+</sup> | 23                |
|         | <i>yap</i> <sup>fu48/+</sup> <i>wwtr1</i> <sup>fu55</sup>   | 13                |
|         | <i>yap</i> <sup>fu48</sup> <i>wwtr1</i> <sup>fu55/+</sup>   | 12                |
|         |   |                   |

Numbers indicate the number of embryos used for the analysis of r5 rhombomeres for Fig. 5.

These findings demonstrated that this effect of TEAD activity on cell proliferation occurred through a cell-autonomous mechanism. Finally, to address whether the Yap/Taz-mediated regulation of boundary cell proliferation impacted on their transition towards the differentiation state, we followed the position of cell clones along the apicobasal axis upon clonal inactivation of Yap/Taz. No changes in the position of the clones were observed, and most of the cells were located in the ventricular zone [Fig. 5J; 94.52% (UAS:DsRed-YapDN) 92.71% (UAS:DsRed-TEAD-DN) versus 92.43% (control UAS:DsRed)]. This result suggested that Yap/Taz-activity was not involved in transitioning cells to differentiation but instead mainly controlled the proliferative state of the progenitors. In line with this finding, no differences were observed when the number of differentiated cells was compared between UAS:DsRed and UAS:DsRed-TEAD-DN clones at 48 hpf [Fig. 5K; 72% (UAS:DsRed-TEAD-DN) versus 83% (control UAS:DsRed) of cells in the HuC-domain]. The combined results demonstrated that Yap and Taz are mechanotransducers that regulate the homeostasis of the progenitor pool in the hindbrain boundaries.

## DISCUSSION

In this study, we provide evidence that mechanical inputs lead to Yap/Taz activity at hindbrain boundaries, which are sites of high mechanical stress during tissue segmentation. Yap and Taz transduce physical properties of the microenvironment into crucial cell decisions, e.g. whether to remain undifferentiated or to maintain the proliferating progenitor pool.

We showed that Yap/Taz activity is confined to the hindbrain boundaries by using the Tg[4xGTTC:GFP] transgenic line as a TEAD-activity reporter. The expression of the transgene not only overlapped with Yap and Taz proteins within the boundaries, but it also matched with the expression pattern in hindbrain boundaries of the newly reported zebrafish TEAD reporter line Tg[Hsa.CTGF:nlsMCherry], which has been described as a bona fide Yap1/Taz reporter (Astone et al., 2018). The expression of Hsa.CTGF:nlsMCherry in the boundaries suggests that *ctgf* could be one of the targets of the TEAD pathway. However, further work is required to reveal the putative TEAD targets within the hindbrain. We show that actomyosin-generated tension in boundary cells is most probably the trigger of Yap/Taz-TEAD activity in this cell population in zebrafish embryos. As amniote embryos do not display actomyosin structures in the hindbrain boundaries (Letelier et al., 2018), the mechanism controlling the proliferative capacity of those boundary cells might be different, as might the mechanism(s) controlling the distinct proliferative capacity of boundaries and rhombomeric regions.

Although rhombomeres rather than boundaries have been described as functioning as centers of cell proliferation in the chick (Guthrie et al., 1991), other studies have proposed that boundaries serve as repetitive pools of stem-like cells at stages when rhombomeres are actively differentiating (Peretz et al., 2016). Here, we demonstrated using several means that boundary cells actively proliferate at early developmental stages in zebrafish embryos, and, at 26 hpf, they exhibit a proliferative behavior that is distinct from that of their rhombomeric neighbors, which were engaged in massive neurogenesis at a much earlier stage (Nikolaou et al., 2009). In this respect, it is interesting that, when cell proliferation was assayed in HH18 chick embryos (at stages when neuronal differentiation is triggered in boundary cells), the ratio of proliferating cells in rhombomeric versus boundary regions was 4:1 (Peretz et al., 2016). We found that this ratio was 1:2 in zebrafish embryos before neuronal differentiation took place in the hindbrain

boundaries in zebrafish (26 hpf), indicating that boundary cells proliferated at a higher rate than rhombomeric cells at this time point. Later on, at the onset of neuronal differentiation within the boundaries (40 hpf), this ratio decreased to 1:1, coinciding with the massive growth of the neuronal differentiation domain observed from 40 hpf onwards (Fig. 4). These findings suggest that boundary territories change from territories that function as an expanding pool of progenitor cells to territories in which there is an equal level of non-boundary proliferative activity and neurogenic capacity. We consider that the different observations in chick and zebrafish can be explained by the different organization of neurogenesis in these two species (Chandrasekhar et al., 1997; Trevarrow et al., 1990). Thus, zebrafish develops much faster than chick: a delay of only 24–28 h is observed between hindbrain segmentation (12 hpf) and neuronal differentiation in boundaries (40 hpf) in zebrafish, whereas this delay is 40 h in the chick (from HH9.5 to HH18). Therefore, as boundary cells undergo neuronal differentiation earlier in zebrafish than in chick, the zebrafish progenitor pool needs to be expanded in order to maintain the homeostasis and growth of the boundaries. This expansion is driven by Yap/Taz-TEAD activity. In this line, it has recently been reported that mechanical forces are overarching regulators of Yap/Taz in multicellular contexts for the control of organ growth (Aragona et al., 2013).

To shed light on the mechanism(s) that boundary cells use for their functional transitions, we focused on how they switch from the proliferative progenitor cell state to differentiated neurons. We generated important insights regarding the cellular/population dynamics and lineage relationships of the Yap/Taz-TEAD active cells and observed that boundary cells dramatically diminished their proliferative activity from 40 hpf onwards, coinciding with the downregulation of Yap/Taz-TEAD activity. Yap and Taz have been considered as gatekeepers of progenitor activity in other systems. For example, Yap and Taz are typically found in the nucleus in somatic stem cells or progenitors, where they have been proposed to function as determinants of a stem cell state (Pancier et al., 2016) or as being instrumental for the crucial expansion of early progenitor populations in the primitive mesenchyme and in overall gut mesenchymal growth (Cotton et al., 2017). In accordance with those reports, the results of our functional approaches indicated that indeed Yap/Taz-TEAD activity maintains the boundary cells in the progenitor state by controlling their proliferative activity and they suggest that levels of mechanical tension and cytoskeletal organization in boundary territories reach the threshold required to activate the transcriptional effects of Yap and Taz. Continued Yap/Taz-TEAD activity would maintain boundary cells in the proliferative progenitor state, and this state would continue until Yap/Taz-TEAD activity ceased. Thus, the demonstration that Yap/Taz mechanotransduction can orient cell behavior in hindbrain boundaries highlights the importance of coordinating morphogenesis and cell fate. In line with this notion, it has been proposed that mechanoactivation of Yap/Taz promotes epidermal stemness in somatic stem cells by regulating Notch (Totaro et al., 2017).

In other systems, Yap appears to be the main regulator of TEAD-dependent cell functions. For example, during optic vesicle development, the fate of retinal pigmented epithelium (RPE) is compromised in *yap*<sup>-/-</sup> zebrafish embryos, whereas *wwtr1*<sup>-/-</sup> embryos develop a normal RPE (Miesfeld et al., 2015). However, in our study hindbrain boundary proliferative behavior was not affected in either *yap*<sup>fu48</sup> or *wwtr1*<sup>fu55</sup> embryos, or in Yap or Taz morphants, suggesting that the two transcriptional co-activators function redundantly. The reasons why such redundant activity is important for maintaining TEAD-activity are currently unclear.

However, one plausible explanation is that such redundancy confers robustness to the system, which may be needed because the expansion of the progenitor pool might be a key requirement for the cell population before becoming a proneural cluster domain.

Our results demonstrate that hindbrain boundary cells in zebrafish give rise to two different derivatives: progenitor cells that are maintained in the ventricular zone and differentiated neurons. It might be interesting to speculate that the cells of this remaining boundary progenitor cell population may behave as long-lasting progenitors that could be used for development and maturation, or that could be recruited for later events of central nervous system growth or repair.

## MATERIALS AND METHODS

### Fish samples

Animals were treated according to the Spanish/European regulations for the handling of animals in research. All protocols were approved by the Institutional Animal Care and Use Ethic Committees of the Barcelona Biomedical Research Park and implemented according to European regulations. All experiments were carried out in accordance with the principles of the 3Rs.

Zebrafish (*Danio rerio*) embryos were obtained by mating of adult fish using standard methods. All zebrafish strains were maintained individually as inbred lines. Two transgenic lines were used for repairing rhombomeres 3 and 5: Mü4127, which is an enhancer trap line in which the trap *KalTA4-UAS-mCherry* cassette was inserted into the 1.5 kb region downstream of *egr2a/krx20* (Distel et al., 2009); and Tg[elA:GFP], which is a stable reporter line in which the chicken element A from *egr2a* was cloned upstream of the *gfp* reporter (Labalette et al., 2011). The Tg[neurog1:DsRed] (Drerup and Nechiporuk, 2013) and Tg[atoh1a:KalTA4;UAS:GFP] (Distel et al., 2010) lines label *neurog1*- or *atoh1a*-cells and their derivatives, respectively. The Tg[HuC:GFP] line labels early differentiated neurons (Park et al., 2000). The mutant lines *yap*<sup>fu48</sup> and *wwtr1*<sup>fu55</sup> were generated using TALEN-induced mutagenesis strategy (Dingare et al., 2018).

### Transgenesis

The Tg[4xGTIIC:d2GFP] line (called Tg[4xGTIIC:GFP] throughout the manuscript) monitors Yap/Taz-TEAD activity (Miesfeld and Link, 2014), and was generated by injecting one-cell stage embryos with the 4xGTIIC:d2GFP construct. The Tg[4xGTIIC:Gal4;UAS:KAED] line was generated by injecting Tg[UAS:KAED] embryos with the 4xGTIIC:Gal4 vector, which was assembled using the Gateway technology (Life Technologies) and the Tol2 kit (Kwan et al., 2007). The 4xGTIIC promoter (Miesfeld and Link, 2014) was placed upstream of Gal4FF. One-cell stage embryos were co-injected with 17.5 ng/μl of Tol2 transposase mRNA and 15 ng/μl of phenol:chloroform-purified 4xGTIIC:Gal4 construct, in a total volume of 2 nl. Three or more stable transgenic lines deriving from different founders were generated. The mutant lines *yap*<sup>fu48</sup> and *wwtr1*<sup>fu55</sup> were crossed with Tg[4xGTIIC:d2GFP] fish in order to have *yap wwtr1* compound mutants within the Yap/Taz-TEAD activity background.

### Cell segmentation

For manual segmentation of single cells, ITK-Snap software was used on embryos from Tg[CAAX:GFP]×Mü4127 crosses (Fig. S1). Single cells located either at the boundary or in the center of the rhombomere were segmented, and the resulting .vtk files were used to display them in the FIJI-3D viewer.

### Whole-mount *in situ* hybridization

Zebrafish whole-mount *in situ* hybridization was adapted from Thisse et al. (1993). The following riboprobes were generated by *in vitro* transcription from cloned cDNAs: *gfp*, *hoxb1a* and *egr2a* (Calzolari et al., 2014), and *rflng* (Cheng et al., 2004). *myl7* and *epha4* probes were generated by PCR amplification (*myl7* Fw primer, 5'-GAC CAA CAG CAA AGC AGA CA-3'; *myl7* Rev primer, 5'-TAA TAC GAC TCA CTA TAG GGT AGG GGG CAG TTA CAG-3'; *epha4* Fw primer, 5'-AAG GAG CTA ACT CCA CCG TGC TC-3'; *epha4* Rev primer, 5'-TAA TAC GAC TCA CTA TAG GGA

GAC ATC TGG GTC TTC CTC CAA A-3') using 24 hpf embryos cDNA. The T7 polymerase binding site was added at the 5' end of the reverse primers and amplification was followed by RNA transcription. The chromogenic *in situ* hybridization was developed using NBT/BCIP (blue) and FastRed (red) substrates. For fluorescent *in situ* hybridization, DIG-labeled riboprobes were developed with fluorescein-tyramide substrate (TSA system). After staining, embryos were either flat-mounted and imaged using a Leica DM6000B fluorescence microscope or were whole-mounted in agarose and imaged using an SP8 Leica confocal microscope.

### BrdU experiments and TUNEL assay

Embryos were incubated with 10 µg/µl 5-bromo-2'-deoxyuridine (Aldrich) for 2 h prior to fixation. Subsequently they were incubated in 2 N HCl for 30 min, washed three times in sodium borate (pH 8.9) and processed for immunohistochemistry. The anti-BrdU BMC9318 antibody (Roche) was used in whole mount at a 1:200 dilution.

Distribution of apoptotic cells in the overall hindbrain was determined by TdT-mediated dUTP nick-end labeling (TUNEL assay) of the fragmented DNA. Briefly, after *epha4* *in situ* hybridization, embryos were fixed for 30 min with 4% (w/v) paraformaldehyde in PBS-Tween. Embryos were then washed with PBS-Tween before incubation with the TUNEL reaction mixture (Roche) for 1 h at 37°C and subsequent PBS-Tween washes. Fluorescein-labeled deoxynucleotides incorporated in apoptotic cells were visualized using an SP8 Leica confocal microscope.

### In toto embryo immunostaining

For immunostaining, embryos were blocked in 5% goat serum in PBS-Tween20 (PBST) for 1 h at room temperature and then incubated overnight at 4°C with the primary antibody. The primary antibodies used were the following: anti-DsRed (1:500; Clontech), anti-GFP (1:200; Torrey Pines), anti-pH3 (1:200; Upstate), anti-Sox2 (1:200; Abcam), anti-Yap (1:100; Santa Cruz), anti-Taz (1:200; Cell Signaling, D24E4) and anti-Myc (1:200; Clontech). After extensive washing with PBST, embryos were incubated with secondary antibodies conjugated with Alexa Fluor488 or Alexa Fluor555 (1:500; Invitrogen). Either Draq5 (1:2000; Biostatus, DR50200) or DAPI were used to label nuclei. Embryos were flat-mounted or whole-mounted in agarose and imaged under a Leica SP5 or SP8 confocal microscope.

### Photoconversion experiments

Tg[4xGTIIC:Gal4;UAS:KAEDE] embryos at 30 or 48 hpf were anesthetized and mounted dorsally in 1% LMP-agarose. KAEDE<sup>G</sup> was fully photoconverted with UV light ( $\lambda=405$  nm) using a 20× objective in a Leica SP8 system. Upon exposure to UV, light emission from KAEDE protein irreversibly shifts from green to red fluorescence (516 to 581 nm). To ensure that all of the cells within the hindbrain were photoconverted, we performed an accurate analysis using confocal microscopy and *yz* confocal cross-sections. In the case of the photoconversion of single-KAEDE<sup>G</sup> cells, embryos at 30 hpf expressing the mosaic 4xGTIIC:Gal4;UAS:KAEDE transgene were used. In all cases, after photoconversion the embryos were returned to embryo medium containing phenylthiourea (PTU) in a 28.5°C incubator. At 48 hpf or 72 hpf, embryos were mounted dorsally and imaged *in vivo* using a Leica SP8 system using PMT detectors and a 20× objective.

### Pharmacological treatments

Treatments with myosin inhibitors such as *para*-nitroblebbistatin and rockout were applied once the neural tube was already formed to avoid interfering with its early morphogenesis (Calzolari et al., 2014). Thus, embryos at 16 hpf were dechorionated and treated until 22 hpf at 28.5°C with *para*-nitroblebbistatin (50 µM) (Képiró et al., 2014) or rockout (50 µM) (Ernst et al., 2012), or DMSO for control experiments. In Fig. 3K-N, treatment was a bit delayed (19–25 hpf) in order to cover the onset of GFP expression at 25 hpf. After treatment, embryos were fixed in 4% PFA for further analysis.

### Conditional overexpression

The Myc:hsp:Rac3bDN (T71N-mutation) construct was generated using site-directed mutagenesis (QuikChange Site-Directed Mutagenesis Kit,

Stratagene, 200518), and cloned into the MCS of a Tol2-based custom vector containing a heat shock promoter (hsp) and a Myc-tag (Letelier et al., 2018). Tg[4xGTIIC:GFP] embryos were injected at the one-cell stage, grown at 28.5°C and heat-shocked at 14 hpf. All embryos were fixed at 30 hpf to give enough time for the Myc-tagged constructs to be expressed. They were then co-immunostained for Myc and GFP, and imaged. The phenotype was scored by analyzing the number of Myc-positive clones expressed in the hindbrain boundaries that displayed GFP (Fig. 3I) and plotted as percentage of boundary clones expressing Myc and GFP (Yap/Taz-activity).

UAS:DsRed, UAS:DsRed-YapDN or UAS:DsRed-TEAD-DN constructs were injected into Tg[4xGTIIC:Gal4;UAS:KAEDE] embryos at the one-cell stage. The embryos were grown until 34 hpf or 48 hpf, fixed, stained with Draq5 and imaged using a confocal microscope. The size of the clones was analyzed by quantifying the nuclei in the DsRed-positive boundary clones. The position of the clones along the apicobasal axis was analyzed by scoring the number of cells within or without the HuC-positive domain.

### 3D and time imaging

#### Time-lapse movie for *in vivo* analysis of cell divisions in the rhombomeric boundaries

Anesthetized live double transgenic Tg[CAAX:GFP]Mu4127 embryos were embedded in 1% low melting point (LMP) agarose with the hindbrain positioned towards the glass-bottom of the Petri dish in order to achieve a dorsal view using an inverted objective. The video was obtained with an inverted SP5 Leica confocal microscope, and was processed and analyzed using Fiji software (NIH). Experimental parameters for the video were: voxel dimension (nm), x267.8 y267.8 z629.4; time frame, 10 min; total time, 8 h; pinhole, 1 Airy; zoom, 2.8; objective, 20× immersion; NA, 0.70.

#### Single-cell tracking experiments

Embryos were anesthetized using 0.04% MS-222 (Sigma) and mounted in 0.6% LMP-agarose in glass capillaries. Time-lapse imaging was performed at 28.5°C using a Zeiss Lightsheet Z.1 microscope. Tg[4xGTIIC:GFP] embryos were injected with hsp::H2B-RFP or *H2B-mCherry* RNA at the one- to eight-cell stage. Embryos injected with hsp::H2B-RFP were heat-shocked for 20 min 2 h before imaging. The cohort of embryos and datasets used in this study are depicted in Table 1 and Fig. S2. Each dataset corresponds to the imaging of a distinct embryo hindbrain. The videos were analyzed, and cells were manually tracked using Fiji software (NIH). Experimental parameters were: voxel dimension (nm), x235.5 y235.5 z1000; time frame, see Table 1; total time, see Table 1; zoom, 1; objective, 20× water-dipping; NA, 1.

#### Mapping the progenitor and neuronal domains within the hindbrain boundaries

Live Tg[HuC:GFP]xMu4127 embryos were imaged at 26, 40 and 70 hpf using a Leica SP8 confocal microscope. Mu4127 staining was used as a landmark for rhombomeric interfaces. Fiji was used to measure the distance expanding from the apical ventricular zone edge (apical) of the neural tube to the basal mantle zone edge in r3/r4 and r4/r5, and this distance was called apico-basal (AB) length (black circle and dashed line, Fig. 4H). The boundary neuronal domain corresponds to the length encompassing the GFP-expressing territory (dark-gray histogram, Fig. 4G). The boundary progenitor domain corresponds to the length resulting from subtraction of the neuronal length from the total length (light-gray histogram, Fig. 4G). The temporal dynamics of the ratio (neuronal HuC+ AB length)/(total AB length) was plotted and compared with the ratio (neuronal area)/(whole hemisphere area) (Fig. 4H).

The position of the tracked cell nuclei relative to the total AB length was plotted on the top of the progenitor/differentiation map (Fig. 4I). Aiming at displaying the data with anatomical coherence, the ratio (position of the nucleus)/(AB length) was subtracted from 1, meaning that values closer to 1 correspond to the cell position in the apical zone, and thus in the ventricular progenitor domain (Fig. 4I).

#### Antisense morpholinos

For morpholino knockdown, embryos were injected at the one-cell stage with splicing-blocking morpholino oligomers (MOs) obtained from

GeneTools. The MOs used were as follows: MO-p53 (Langheinrich et al., 2002), MO-Yap (Agarwala et al., 2015), MO-Taz (*wnt1* gene; 5'-CTG GAG AGG ATT ACC GCT CAT GGT C-3' and MO-Rac3b [see MO-Rac3bSBI4E5 in Letelier et al. (2018)]. A random 25-nucleotide morpholino was injected as a control. MO-p53 was included in all MO injections to diminish putative artifacts (Gerety and Wilkinson, 2011). Efficiency of the injected morpholinos is displayed in Fig. S3.

## Phenotypic analyses

### Morphant mutants and compound mutants

Apoptotic and cell proliferation analyses were performed in 34 hpf embryos. As boundary cells are located at the interface between adjacent rhombomeres and are composed of two cell-rows, one from each rhombomere (even/odd rhombomeres; Fig. S1B-D''), we used the borders of *epha4* expression in r3 and r5 as boundary landmarks. Fluorescent *in situ* hybridization for *epha4* perfectly corresponded with the edges of rhombomeres, as shown in Fig. S1I-I''. Embryos of distinct genotypes were therefore fixed with 4% PFA and assayed for *epha4* *in situ* hybridization prior to cell proliferation or apoptosis analyses. The last row of *epha4*-negative cells and the first row of *epha4*-positive cells (or the other way around depending on the interface) constitute the boundary cell population. Hence, *in situ* hybridization for *epha4* allows the localization of r2/r3, r3/r4, r4/r5 and r5/r6 boundaries. Embryos were imaged under the Leica SP8 confocal microscope. Apoptotic (TUNEL) and proliferating (pH3-expressing) boundary cells were quantified at r3/r4 and r4/r5 boundaries, whereas r5 was the rhombomeric territory used for non-boundary cell population analysis.

### Clonal analysis

Injected embryos were fixed with 4% PFA and stained using Draq5. The size of each clone in the boundaries was assessed by quantifying the number of DsRed-positive nuclei at 34 hpf. Cell fate was analyzed according to cell position in the neural tube, where progenitor cells are those cells in contact with the ventricle. The percentage of ventricular cells per clone at 34 hpf was plotted. For cell differentiation analysis, injected embryos were fixed at 48 hpf and immunostained for HuC; cells displaying DsRed and HuC were quantified.

### Acknowledgements

We are grateful to the referees whose insights improved our paper. We thank Brian Link who kindly provided us with constructs and reagents. We also thank S Calatayud, L Subirana and M Linares for technical assistance, and the members of Pujades lab for critical insights.

### Competing interests

The authors declare no competing or financial interests.

### Author contributions

Conceptualization: A.V., C.P.; Methodology: A.V., C.F.H., C.E.-P.; Validation: A.V., C.F.H., C.E.-P., C.P.; Formal analysis: A.V., C.N., C.P.; Investigation: A.V., C.F.H., C.E.-P.; Resources: C.D., S.C., J.T., C.N., V.L.; Data curation: A.V., C.P.; Writing - original draft: C.P.; Writing - review & editing: C.P.; Supervision: C.P.; Project administration: C.P.; Funding acquisition: C.P.

### Funding

This work was supported by a La Marató-TV3 grant (345/C/2014) and by a Ministerio de Ciencia, Innovación y Universidades grant (BFU2015-67400-P and BFU2016-81887-REDT/AEI) to C.P.; and by a Unidad de Excelencia María de Maetzu grant (MDM-2014-0370) to the Department of Experimental and Health Sciences of the Pompeu Fabra University (DCEXS-UPF). A.V. was a recipient of a predoctoral fellowship from the Fundació La Caixa, and C.E.-P. holds a predoctoral fellowship from the Ministerio de Ciencia, Innovación y Universidades (FPU). J.T. was a recipient of a postdoctoral Beatriu de Pinos fellowship (AGAUR, Generalitat de Catalunya). C.P. is recipient of an Institució Catalana per la Recerca i Estudis Avançats Academia award (Generalitat de Catalunya).

### Supplementary information

Supplementary information available online at <http://dev.biologists.org/lookup/doi/10.1242/dev.176735.supplemental>

## References

- Agarwala, S., Duquesne, S., Liu, K., Boehm, A., Grimm, L., Link, S., König, S., Eimer, S., Ronneberger, O. and Lecaudey, V. (2015). Amotl2a interacts with the Hippo effector Yap1 and the Wnt/ $\beta$ -catenin effector Lef1 to control tissue size in zebrafish. *Elife* **4**, e08201. doi:10.7554/eLife.08201
- Ando, R., Hama, H., Yamamoto-Hino, M., Mizuno, H. and Miyawaki, A. (2002). An optical marker based on the UV-induced green-to-red photoconversion of a fluorescent protein. *Proc. Natl Acad. Sci. USA* **99**, 12651-12656. doi:10.1073/pnas.202320599
- Aragona, M., Panciera, T., Manfrin, A., Giullitti, S., Michielin, F., Elvassore, N., Dupont, S. and Piccolo, S. (2013). A mechanical checkpoint controls multicellular growth through YAP/TAZ regulation by actin-processing factors. *Cell* **154**, 1047-1059. doi:10.1016/j.cell.2013.07.042
- Astone, M., Lai, J. K. H., Dupont, S., Stainier, D. Y. R., Argenton, F. and Vettori, A. (2018). Zebrafish mutants and TEAD reporters reveal essential functions for Yap and Taz in posterior cardinal vein development. *Sci. Rep.* **8**, 10189. doi:10.1038/s41598-018-27657-x
- Benham-Pyle, B. W., Pruitt, B. L. and Nelson, W. J. (2015). Cell adhesion. Mechanical strain induces E-cadherin-dependent Yap1 and  $\beta$ -catenin activation to drive cell cycle entry. *Science* **348**, 1024-1027. doi:10.1126/science.aaa4559
- Calvo, F., Ege, N., Grande-Garcia, A., Hooper, S., Jenkins, R. P., Chaudhry, S. I., Harrington, K., Williamson, P., Moeendarbary, E., Charras, G. et al. (2013). Mechanotransduction and YAP-dependent matrix remodelling is required for the generation and maintenance of cancer-associated fibroblasts. *Nat. Cell Biol.* **15**, 637-646. doi:10.1038/ncb2756
- Calzolari, S., Terriente, J. and Pujades, C. (2014). Cell segregation in the vertebrate hindbrain relies on actomyosin cables located at the interhomomeric boundaries. *EMBO J.* **33**, 686-701. doi:10.1002/emboj.201386003
- Chandrasekhar, A., Moens, C. B., Warren, J. T., Kimmel, C. B. and Kuwada, J. Y. (1997). Development of branchiomotor neurons in zebrafish. *Development* **124**, 2633-2644.
- Chaudhuri, O., Gu, L., Klumpers, D., Darnell, M., Bencherif, S. A., Weaver, J. C., Huebsch, N., Lee, H.-P., Lippens, E., Duda, G. N. et al. (2016). Hydrogels with tunable stress relaxation regulate stem cell fate and activity. *Nat. Mater.* **15**, 326-334. doi:10.1038/nmat4489
- Cheng, Y.-C., Amoyel, M., Qiu, X., Jiang, Y.-J., Xu, Q. and Wilkinson, D. G. (2004). Notch activation regulates the segregation and differentiation of rhombomere boundary cells in the zebrafish hindbrain. *Dev. Cell* **6**, 539-550. doi:10.1016/S1534-5807(04)00097-8
- Cooke, J. E., Kemp, H. A. and Moens, C. B. (2005). EphA4 is required for cell adhesion and rhombomere-boundary formation in the zebrafish. *Curr. Biol.* **15**, 536-542. doi:10.1016/j.cub.2005.02.019
- Cotton, J. L., Li, Q., Ma, L., Park, J.-S., Wang, J., Ou, J., Zhu, L. J., Ip, Y. T., Johnson, R. L. and Mao, J. (2017). YAP/TAZ and hedgehog coordinate growth and patterning in gastrointestinal mesenchyme. *Dev. Cell* **43**, 35-47.e4. doi:10.1016/j.devcel.2017.08.019
- Dingare, C., Niedzwetzki, A., Klemmt, P. A., Godbersen, S., Fuentes, R., Mullins, M. C. and Lecaudey, V. (2018). The Hippo pathway effector Taz is required for cell morphogenesis and fertilization in zebrafish. *Development* **145**, dev167023. doi:10.1242/dev.167023
- Distel, M., Wullmann, M. F. and Köster, R. W. (2009). Optimized Gal4 genetics for permanent gene expression mapping in zebrafish. *Proc. Natl. Acad. Sci. USA* **106**, 13365-13370. doi:10.1073/pnas.0903060106
- Distel, M., Hocking, J. C., Volkman, K. and Köster, R. W. (2010). The centrosome neither persistently leads migration nor determines the site of axonogenesis in migrating neurons in vivo. *J. Cell Biol.* **191**, 875-890. doi:10.1083/jcb.201004154
- Drerup, C. M. and Nechiporuk, A. V. (2013). JNK-interacting protein 3 mediates the retrograde transport of activated c-Jun N-terminal kinase and lysosomes. *PLoS Genet.* **9**, e1003303. doi:10.1371/journal.pgen.1003303
- Dupont, S., Morsut, L., Aragona, M., Enzo, E., Giullitti, S., Cordenonsi, M., Zanconato, F., Le Digabel, J., Forcato, M., Bicciato, S. et al. (2011). Role of YAP/TAZ in mechanotransduction. *Nature* **474**, 179-183. doi:10.1038/nature10137
- Elosegui-Artola, A., Oriá, R., Chen, Y., Kosmalka, A., Pérez-González, C., Castro, N., Zhu, C., Trepats, X. and Roca-Cusachs, P. (2016). Mechanical regulation of a molecular clutch defines force transmission and transduction in response to matrix rigidity. *Nat. Cell Biol.* **18**, 540-548. doi:10.1038/ncb3336
- Elosegui-Artola, A., Andreu, I., Beedle, A. E. M., Lezamiz, A., Uroz, M., Kosmalka, A. J., Oriá, R., Kechagia, J. Z., Rico-Lastres, P., Le Roux, A.-L. et al. (2017). Force triggers YAP nuclear entry by regulating transport across nuclear pores. *Cell* **171**, 1397-1410.e14. doi:10.1016/j.cell.2017.10.008
- Ernst, S., Liu, K., Agarwala, S., Moratscheck, N., Avci, M. E., Dalle Nogare, D., Chitnis, A. B., Ronneberger, O. and Lecaudey, V. (2012). Shroom3 is required downstream of FGF signalling to mediate proneuroblast assembly in zebrafish. *Development* **139**, 4571-4581. doi:10.1242/dev.083253
- Fraser, S., Keynes, R. and Lumsden, A. (1990). Segmentation in the chick embryo hindbrain is defined by cell lineage restrictions. *Nature* **344**, 431-435. doi:10.1038/344431a0

- Fukui, H., Terai, K., Nakajima, H., Chiba, A., Fukuhara, S. and Mochizuki, N. (2014). S1P-Yap1 signaling regulates endoderm formation required for cardiac precursor cell migration in zebrafish. *Dev. Cell* **31**, 128-136. doi:10.1016/j.devcel.2014.08.014
- Galant, S., Furlan, G., Coolen, M., Dirian, L., Foucher, I. and Bally-Cuif, L. (2016). Embryonic origin and lineage hierarchies of the neural progenitor subtypes building the zebrafish adult midbrain. *Dev. Biol.* **420**, 120-135. doi:10.1016/j.ydbio.2016.09.022
- Gerety, S. S. and Wilkinson, D. G. (2011). Morpholino artifacts provide pitfalls and reveal a novel role for pro-apoptotic genes in hindbrain boundary development. *Dev. Biol.* **350**, 279-289. doi:10.1016/j.ydbio.2010.11.030
- Guthrie, S. and Lumsden, A. (1991). Formation and regeneration of rhombomere boundaries in the developing chick hindbrain. *Development* **112**, 221-229.
- Guthrie, S., Butcher, M. and Lumsden, A. (1991). Patterns of cell division and interkinetic nuclear migration in the chick embryo hindbrain. *J. Neurobiol.* **22**, 742-754. doi:10.1002/neu.480220709
- Gutzman, J. H. and Sive, H. (2010). Epithelial relaxation mediated by the myosin phosphatase regulator Mypt1 is required for brain ventricle lumen expansion and hindbrain morphogenesis. *Development* **137**, 795-804. doi:10.1242/dev.042705
- Halder, G., Dupont, S. and Piccolo, S. (2012). Transduction of mechanical and cytoskeletal cues by YAP and TAZ. *Nat. Rev. Mol. Cell Biol.* **13**, 591-600. doi:10.1038/nrm3416
- Hatta, K., Tsujii, H. and Omura, T. (2006). Cell tracking using a photoconvertible fluorescent protein. *Nat. Protoc.* **1**, 960-967. doi:10.1038/nprot.2006.96
- Hiscock, T. W., Miesfeld, J. B., Mosaliganti, K. R., Link, B. A. and Megason, S. G. (2018). Feedback between tissue packing and neurogenesis in the zebrafish neural tube. *Development* **145**, dev157040. doi:10.1242/dev.157040
- Jimenez-Guri, E., Udina, F., Colas, J.-F., Sharpe, J., Padrón-Barthe, L., Torres, M. and Pujades, C. (2010). Clonal analysis in mice underlines the importance of rhombomeric boundaries in cell movement restriction during hindbrain segmentation. *PLoS ONE* **5**, e10112. doi:10.1371/journal.pone.0010112
- Képiró, M., Várkuti, B. H., Végner, L., Vörös, G., Hegyi, G., Varga, M. and Málnási-Csizmadia, A. (2014). para-Nitroblebbistatin, the non-cytotoxic and photostable myosin II inhibitor. *Angew. Chem. Int. Ed. Engl.* **53**, 8211-8215. doi:10.1002/anie.201403540
- Kiecker, C. and Lumsden, A. (2005). Compartments and their boundaries in vertebrate brain development. *Nat. Rev. Neurosci.* **6**, 553-564. doi:10.1038/nrn1702
- Kwan, K. M., Fujimoto, E., Grabher, C., Mangum, B. D., Hardy, M. E., Campbell, D. S., Parant, J. M., Yost, H. J., Kanki, J. P. and Chien, C.-B. (2007). The Tol2kit: a multisite gateway-based construction kit for Tol2 transposon transgenesis constructs. *Dev. Dyn.* **236**, 3088-3099. doi:10.1002/dvdy.21343
- Labalette, C., Bouchoucha, Y. X., Wassef, M. A., Gongal, P. A., Le Men, J., Becker, T., Gilardi-Hebenstreit, P. and Charnay, P. (2011). Hindbrain patterning requires fine-tuning of early *krox20* transcription by *Sprouty 4*. *Development* **138**, 317-326. doi:10.1242/dev.057299
- Langheinrich, U., Hennen, E., Stott, G. and Vacun, G. (2002). Zebrafish as a model organism for the identification and characterization of drugs and genes affecting p53 signaling. *Curr. Biol.* **12**, 2023-2028. doi:10.1016/S0960-9822(02)01319-2
- Letelier, J., Terriente, J., Belzunce, I., Voltas, A., Undurraga, C. A., Polvillo, R., Devos, L., Tena, J. J., Maeso, I., Rétaux, S. et al. (2018). Evolutionary emergence of the *rac3b/rfng/sgca* regulatory cluster refined mechanisms for hindbrain boundaries formation. *Proc. Natl. Acad. Sci. USA* **115**, E3731-E3740. doi:10.1073/pnas.1719885115
- Maves, L., Jackman, W. and Kimmel, C. B. (2002). FGF3 and FGF8 mediate a rhombomere 4 signaling activity in the zebrafish hindbrain. *Development* **129**, 3825-3837.
- Miesfeld, J. B. and Link, B. A. (2014). Establishment of transgenic lines to monitor and manipulate Yap/Taz-Tead activity in zebrafish reveals both evolutionarily conserved and divergent functions of the Hippo pathway. *Mech. Dev.* **133**, 177-188. doi:10.1016/j.mod.2014.02.003
- Miesfeld, J. B., Gestri, G., Clark, B. S., Flinn, M. A., Poole, R. J., Bader, J. R., Besharse, J. C., Wilson, S. W. and Link, B. A. (2015). Yap and Taz regulate retinal pigment epithelial cell fate. *Development* **142**, 3021-3032. doi:10.1242/dev.119008
- Nakayama, Y., Inomata, C., Yuikawa, T., Tsuda, S. and Yamasu, K. (2017). Comprehensive analysis of target genes in zebrafish embryos reveals *gbx2* involvement in neurogenesis. *Dev. Biol.* **430**, 237-248. doi:10.1016/j.ydbio.2017.07.015
- Nikolaou, N., Watanabe-Asaka, T., Gerety, S., Distel, M., Köster, R. W. and Wilkinson, D. G. (2009). Lunatic fringe promotes the lateral inhibition of neurogenesis. *Development* **136**, 2523-2533. doi:10.1242/dev.034736
- Panciera, T., Azzolin, L., Fujimura, A., Di Biagio, D., Frasson, C., Bresolin, S., Soligo, S., Basso, G., Biccato, S., Rosato, A., et al. (2016). Induction of expandable tissue-specific stem/progenitor cells through transient expression of YAP/TAZ. *Cell stem cell*, **19**, 725-737. doi:10.1016/j.stem.2016.08.009
- Panciera, T., Azzolin, L., Cordenonsi, M. and Piccolo, S. (2017). Mechanobiology of YAP and TAZ in physiology and disease. *Nat. Rev. Mol. Cell Biol.* **18**, 758-770. doi:10.1038/nrm.2017.87
- Park, H.-C., Kim, C.-H., Bae, Y.-K., Yeo, S.-Y., Kim, S.-H., Hong, S.-K., Shin, J., Yoo, K.-W., Hibi, M., Hirano, T. et al. (2000). Analysis of upstream elements in the HuC promoter leads to the establishment of transgenic zebrafish with fluorescent neurons. *Dev. Biol.* **227**, 279-293. doi:10.1006/dbio.2000.9898
- Peretz, Y., Eren, N., Kohl, A., Hen, G., Yaniv, K., Weisinger, K., Cinnamon, Y. and Sela-Donenfeld, D. (2016). A new role of hindbrain boundaries as pools of neural stem/progenitor cells regulated by *Sox2*. *BMC Biol.* **14**, 57. doi:10.1186/s12915-016-0277-y
- Riley, B. B., Chiang, M.-Y., Storch, E. M., Heck, R., Buckles, G. R. and Lekven, A. C. (2004). Rhombomere boundaries are Wnt signaling centers that regulate metamer patterning in the zebrafish hindbrain. *Dev. Dyn.* **231**, 278-291. doi:10.1002/dvdy.20133
- Sapède, D., Dyballa, S. and Pujades, C. (2012). Cell lineage analysis reveals three different progenitor pools for neurosensory elements in the otic vesicle. *J. Neurosci.* **32**, 16424-16434. doi:10.1523/JNEUROSCI.3686-12.2012
- Terriente, J., Gerety, S. S., Watanabe-Asaka, T., Gonzalez-Quevedo, R. and Wilkinson, D. G. (2012). Signalling from hindbrain boundaries regulates neuronal clustering that patterns neurogenesis. *Development* **139**, 2978-2987. doi:10.1242/dev.080135
- Thisse, C., Thisse, B., Schilling, T. F. and Postlethwait, J. H. (1993). Structure of the zebrafish *snail1* gene and its expression in wild-type, spadetail and no tail mutant embryos. *Development* **119**, 1203-1215.
- Totaro, A., Castellani, M., Battilana, G., Zanonato, F., Azzolin, L., Giulitti, S., Cordenonsi, M. and Piccolo, S. (2017). YAP/TAZ link cell mechanics to Notch signalling to control epidermal stem cell fate. *Nat. Commun.* **8**, 15206. doi:10.1038/ncomms15206
- Trearrow, B., Marks, D. L. and Kimmel, C. B. (1990). Organization of hindbrain segments in the zebrafish embryo. *Neuron* **4**, 669-679. doi:10.1016/0896-6273(90)90194-K
- Wada, K.-I., Itoga, K., Okano, T., Yonemura, S. and Sasaki, H. (2011). Hippo pathway regulation by cell morphology and stress fibers. *Development* **138**, 3907-3914. doi:10.1242/dev.070987
- Zhao, B., Ye, X., Yu, J., Li, L., Li, W., Li, S., Yu, J., Lin, J. D., Wang, C.-Y., Chinnaiyan, A. M. et al. (2008). TEAD mediates YAP-dependent gene induction and growth control. *Genes Dev.* **22**, 1962-1971. doi:10.1101/gad.1664408